Metastasis-suppressor NME1 controls the invasive switch of breast cancer by regulating MT1-MMP surface clearance

Catalina Lodillinsky, Laetitia Fuhrmann, Marie Irondelle, Olena Pylypenko, Xiao-Yan Li, Hélène Bonsang-Kitzis, Fabien Reyal, Sophie Vacher, Claire Calmel, Olivier de Wever, et al.

Oncogene
https://doi.org/10.1038/s41388-021-01826-1

ARTICLE

Metastasis-suppressor NME1 controls the invasive switch of breast cancer by regulating MT1-MMP surface clearance

Catalina Lodillinsky[1,2] · Laetitia Fuhrmann[3] · Marie Irondelle[4] · Olena Pylypenko[4] · Xiao-Yan Li[5] · Hélène Bonsang-Kitzis[6,7,12] · Fabien Reyal[6,7] · Sophie Vacher[8] · Claire Calmel[9] · Olivier De Wever[10] · Ivan Bièche[8] · Marie-Lise Lacombe[9] · Ana Maria Eiján[1,2] · Anne Houdusse[4] · Anne Vincent-Salomon[3] · Stephen J. Weiss[5] · Philippe Chavrier[4] · Mathieu Boissan[9,11]

Received: 7 October 2020 / Revised: 13 April 2021 / Accepted: 27 April 2021

Abstract

Membrane Type 1 Matrix Metalloprotease (MT1-MMP) contributes to the invasive progression of breast cancers by degrading extracellular matrix tissues. Nucleoside diphosphate kinase, NME1/NM23-H1, has been identified as a metastasis suppressor; however, its contribution to local invasion in breast cancer is not known. Here, we report that NME1 is up-regulated in ductal carcinoma in situ (DCIS) as compared to normal breast epithelial tissues. NME1 levels drop in microinvasive and invasive components of breast tumor cells relative to synchronous DCIS foci. We find a strong anti-correlation between NME1 and plasma membrane MT1-MMP levels in the invasive components of breast tumors, particularly in aggressive histological grade III and triple-negative breast cancers. Knockout of NME1 accelerates the invasive transition of breast tumors in the intraductal xenograft model. At the mechanistic level, we find that MT1-MMP, NME1 and dynamin-2, a GTPase known to require GTP production by NME1 for its membrane fission activity in the endocytic pathway, interact in clathrin-coated vesicles at the plasma membrane. Loss of NME1 function increases MT1-MMP surface levels by inhibiting endocytic clearance. As a consequence, the ECM degradation and invasive potentials of breast cancer cells are enhanced. This study identifies the down-modulation of NME1 as a potent driver of the in situ-to invasive transition during breast cancer progression.

Introduction

Ductal carcinoma in situ (DCIS) correspond to the proliferation of neoplastic breast epithelial cells contained within a layer of myoepithelial cells and an intact basement

These authors contributed equally: Philippe Chavrier, Mathieu Boissan.

Supplementary information The online version contains supplementary material available at https://doi.org/10.1038/s41388-021-01826-1.

✉ Mathieu Boissan
mathieu.boissan@inserm.fr

1 Research Area, Instituto de Oncología Ángel H. Roffo, Universidad de Buenos Aires, Buenos Aires, Argentina

2 Consejo Nacional de Investigaciones Científicas y Técnicas (CONICET), Buenos Aires, Argentina

3 Diagnostic and Theranostic Medicine Division, Institut Curie, PSL Research University, Paris, France

4 Institut Curie, CNRS UMR144, PSL Research University, Paris, France

5 Division of Medical Genetics, Department of Internal Medicine, Life Sciences Institute, University of Michigan, Ann Arbor, MI, USA

6 Department of Surgery, Institut Curie, Paris, France

7 Translational Research Department, RT2Lab Team, INSERM U932, Immunity and Cancer, Institut Curie, Paris, France

8 Pharmacogenomic Unit, Institut Curie, Paris, France

9 INSERM UMR_S 938, Saint-Antoine Research Center, CRSA, University Sorbonne, Paris, France

10 Laboratory of Experimental Cancer Research, Cancer Research Institute Ghent (CRIG), Department of Human Structure and Repair, Ghent University, Ghent, Belgium

11 Laboratory of Biochemistry and Hormonology, Tenon Hospital, AP-HP, Paris, France

12 Present address: Gynecological and Breast Surgery and Cancerology Center, RAMSAY-Générale de Santé, Hôpital Privé des Peupliers, Paris, France

Published online: 19 May 2021

membrane [1]. If untreated, some DCIS (20–50%) will progress to invasive breast cancer (IBC) with characteristic tumor cell dissemination and poor outcome [1]. Synchronous adjacent DCIS and IBC foci show similar transcriptomic and genomic profiles, and few progression markers have been identified so far [2, 3]. Thus, a better understanding of the mechanisms and players underlying the progression to the invasive disease is needed in order to improve treatment decision and outcome.

Nucleoside diphosphate kinases (NDPKs), the products of the evolutionary conserved *NME/NM23* gene family, catalyze phosphate transfer from nucleoside triphosphates (mostly ATP) to nucleoside diphosphates [4]. Interestingly, NME1/NM23-H1 has been identified as the first metastasis suppressor, showing reduced expression in highly melanoma metastatic cells and as a suppressor of breast, liver, and colon carcinoma metastasis [5, 6]. At the mechanistic level, mutations in the drosophila *nme* homolog, *abnormal wing discs* (*awd*), are associated with developmental defects, and genetic studies have linked awd with *shibire* (*shi*), the gene encoding dynamin GTPase, required for membrane fission in the endocytic pathway [7]. We recently reported that human NME1 interacts with and supplies dynamin with high GTP levels required for membrane fission and, consequently, promotes endocytosis and clearance of cell surface receptors [8, 9].

A hallmark of metastasis is the acquisition of an invasive program enabling cancer cells to remodel the extracellular matrix (ECM) and disseminate. MT1-MMP (aka MMP-14), a trans-membrane matrix metalloproteinase, is required for DCIS-to-IBC progression and local invasion in the mammary gland. In addition, MT1-MMP up-regulation has been associated with higher metastatic risk in breast cancer [10–13]. It is well established that MT1-MMP is essential for carcinoma cell invasion by allowing the pericellular degradation of basement membrane and collagen-rich interstitial tissue barriers by cancer cells [14, 15]. A balance of endocytic and exocytic fluxes is thought to ensure a constant supply of active MT1-MMP at the plasma membrane [15–19]. MT1-MMP can be efficiently internalized by clathrin-mediated endocytosis and it is essential to better understand the molecular mechanisms that control its clearance from the cell surface.

The metastasis-suppressor role of NME1 together with its promoting function of dynamin activity in endocytosis, as well as the regulation of MT1-MMP surface exposure through endocytosis raise the intriguing possibility of a control of MT1-MMP activity by NME1 NDPK in cancer cells. The potential implication of NME1 and its close relative NME2 protein, during the invasive DCIS-to-IBC switch during breast cancer progression has been overlooked. Here, we investigated the expression of NME1 and NME2 in synchronous DCIS and IBC foci in breast tumors. We found an up-regulation of NME1 in DCIS as compared to normal peritumoral breast tissues and further down-regulation in invasive disease components. NME2 expression, which was similarly up-regulated in DCIS, remained high in IBCs. The ability of NME1 or NME2 to influence tumor invasion was evaluated using the intraductal xenograft model involving the injection of human MCF10DCIS.com cells into the primary duct of mouse mammary glands [11, 20]. Suppression of NME1, but not that of NME2, accelerated the invasive switch of MCF10DCIS.com tumor xenografts in the intraductal injection model. Finally, we found a specific association of NME1 with endocytic clathrin-coated structures and a regulation of MT1-MMP surface levels by dynamin downstream of NME1, clarifying the mechanism underlying the increased invasive potential of breast cancer cells during the DCIS-to-IBC transition.

Experimental procedures

Cell culture

See SI Experimental Procedures.

Materials

For DNA constructs, antibodies, production and purification of recombinant proteins, see SI Experimental Procedures.

RNA interference and CRISPR/Cas9 technology

See SI Experimental Procedures and SI Table S1.

Human breast tumor samples and tissue microarray construction

Approximately 160 samples of primary breast tumors harboring synchronous DCIS and IBC, and 37 microinvasive breast carcinomas were collected at Institut Curie (SI Table S2). Analysis of the human samples by immunohistochemistry was performed, as detailed in SI Experimental Procedures.

Immunohistochemical (IHC) staining of breast tumor tissue microarray

IHC was performed using validated highly selective NME1 and NME2 polyclonal antibodies, as detailed in SI Experimental Procedures.

Unsupervised hierarchical clustering

The membranous H-score of MT1-MMP and the total H-score of NME1 from in situ and infiltrating tumor

samples were scaled and then analyzed by unsupervised hierarchical clustering, as detailed in SI Experimental Procedures.

Intraductal transplantation method

The intraductal xenograft model was carried out as previously described [11, 20]. For details, see SI Experimental Procedures.

Histological and immunofluorescence analysis of mouse tissue sections

See SI Experimental Procedures.

3D collagen I invasion assay, quantification of pericellular collagenolysis, multicellular spheroid outgrowth in 3D matrigel, analysis of MT1-MMP cell surface expression, MT1-MMP internalization

See SI Experimental Procedures.

In situ proximity ligation assay (PLA)

See SI Experimental Procedures.

Immunoprecipitation

See SI Experimental Procedures.

Subcellular fractionation

See SI Experimental Procedures.

Pull-down assay

See SI Experimental Procedures.

Statistical analysis

See SI Experimental Procedures.

Results

Down-regulation of NME1 in microinvasive breast cancers and in IBCs

NME expression was investigated by IHC analysis on whole sections and on a tissue microarray (TMA) of synchronous DCIS and IBC foci from 156 breast cancer patient samples using specific NME1 pAb and NME2 mAb with no cross-reactivity (Supplementary Fig. S1 and Table S2). Contrasting with low or undetectable NME1 levels in healthy breast epithelial cells, NME1 was significantly up-regulated in DCIS cells, in which a strong cytoplasmic and peripheral staining was observed (Fig. 1A–C and E, G and Supplementary Fig. S2). In addition, NME1 levels were lower in IBCs relative to synchronous DCIS foci considering either total or separated cytoplasmic and membranous NME1 staining (Fig. 1D, F, H and Supplementary Fig. S2). When tumors were stratified into luminal A/B, HER2 + and triple-negative breast cancer (TNBC) subtypes, cytoplasmic and membranous NME1 levels remained significantly lower in the invasive component as compared to the adjacent DCIS foci, irrespective of the molecular subtype (Supplementary Fig. S3A–C). In addition, NME1 expression was lower in TNBC relative to luminal tumors, the former being aggressive and poor outcome tumors, irrespective of the in situ or invasive contingents (Supplementary Fig. S3D, E). Identical results were obtained using mouse NME1 mAb (Supplementary Fig. S1A and Fig. S4). Strikingly, NME1 level was also strongly decreased in microinvasive foci (a relatively rare tumor subset corresponding to early loco-regional invasion with no invasive focus > 1 mm [21, 22]), relative to the in situ component from the same specimen (Supplementary Fig. S5). Collectively, these findings indicate that down-regulation of NME1 NDPK correlates with the onset of breast cancer invasion.

NME2 up-regulation during breast cancer progression

NME2 staining using a validated, highly selective mAb (Supplementary Fig. S1B–D) was visible at the apical surface of luminal epithelial cells in normal breast tissues (Supplementary Fig. S6A, B, left row, arrows). Similar to NME1, NME2 cytoplasmic staining was strongly up-regulated in DCIS as compared to adjacent normal cells (Supplementary Fig. S6A, B, middle row and Fig. S6C, E), while there was no difference considering the plasma membrane association of NME2 (Supplementary Fig. S6G). However, in sharp contrast to the drop in NME1 expression in IBCs, NME2 remained elevated in IBCs similar to its levels in DCIS (Supplementary Fig. S6A, B, right row and Fig. S6D, F, H).

Anti-correlation of NME1 and MT1-MMP in breast cancer cells

Given the up-regulation of MT1-MMP during the in situ-to-invasive transition in relation with poor clinical outcome [11], we compared NME1 and MT1-MMP levels in the breast tumor cohort. We observed a striking anti-correlation of cortical MT1-MMP and NME1 both in DCIS and IBC

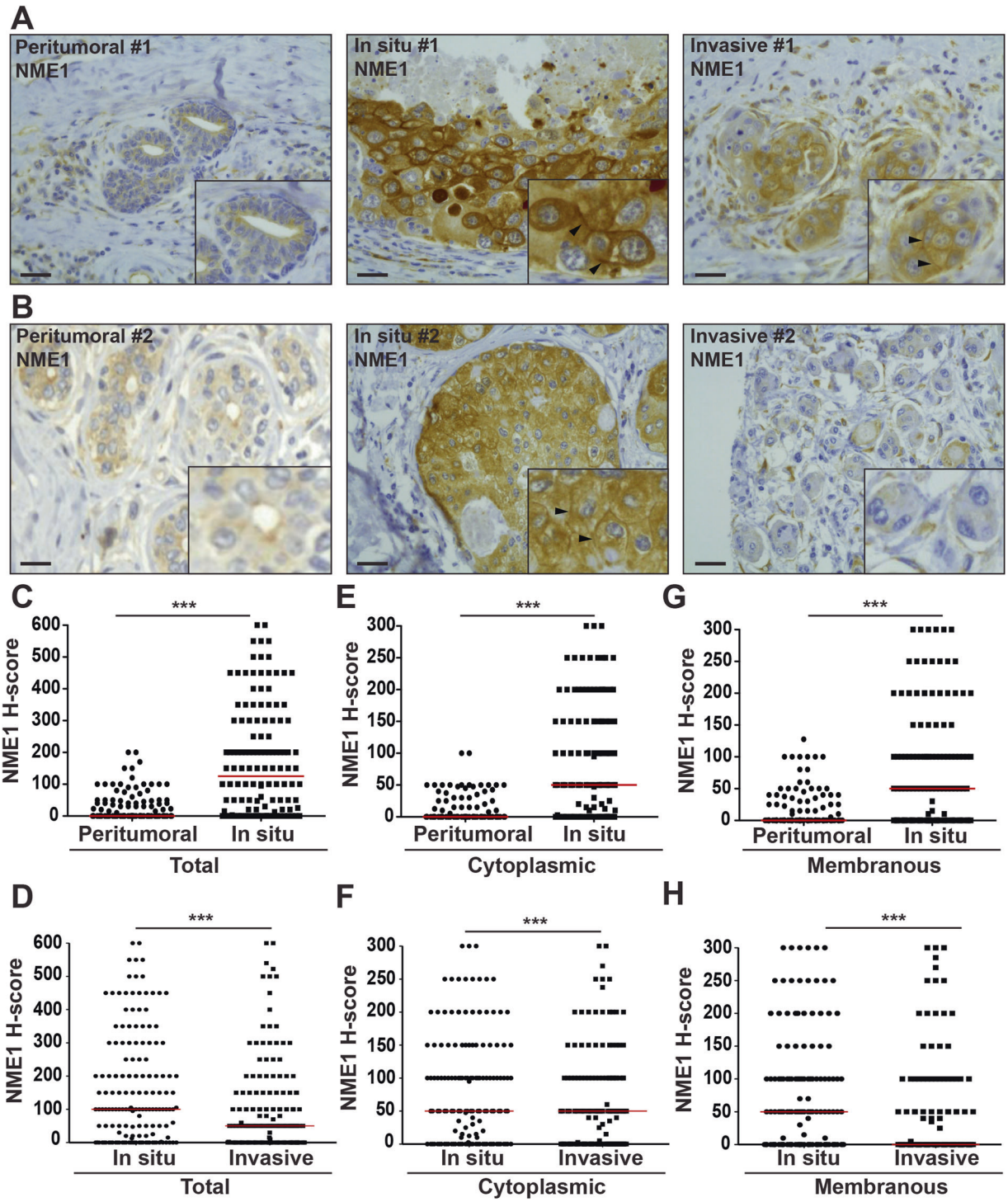

Fig. 1 Biphasic up- and down-modulation of NME1 expression during breast cancer progression. A, **B** Representative NME1 IHC staining in breast peritumoral tissues and synchronous in situ and invasive components from two breast carcinoma biopsies. Arrowheads point to submembranous staining. Scale bar, 25 µm. **C**, **E**, **G** Comparison of total (**C**), cytoplasmic (**E**) and plasma membrane (**G**) NME1 levels using the H-score method in the in situ breast carcinomas as compared to adjacent breast peritumoral tissues. ***$P < 0.001$. **D**, **F**, **H** Total (**D**), cytoplasmic (**F**), and plasma membrane (**H**) NME1 levels were compared in synchronous in situ and invasive components of breast tumor biopsies. ***$P < 0.001$. The median of each H-score distribution is represented (red bar).

breast tumor counterparts (Fig. 2A, B and Supplementary Fig. S7). NME1 and cortical MT1-MMP levels were scaled (Supplementary Fig. S8) and analyzed by unsupervised hierarchical clustering method, confirming the strong anti-correlation between the two proteins both in DCIS and IBC contingents (Fig. 2C–F). Anti-correlation was observed in

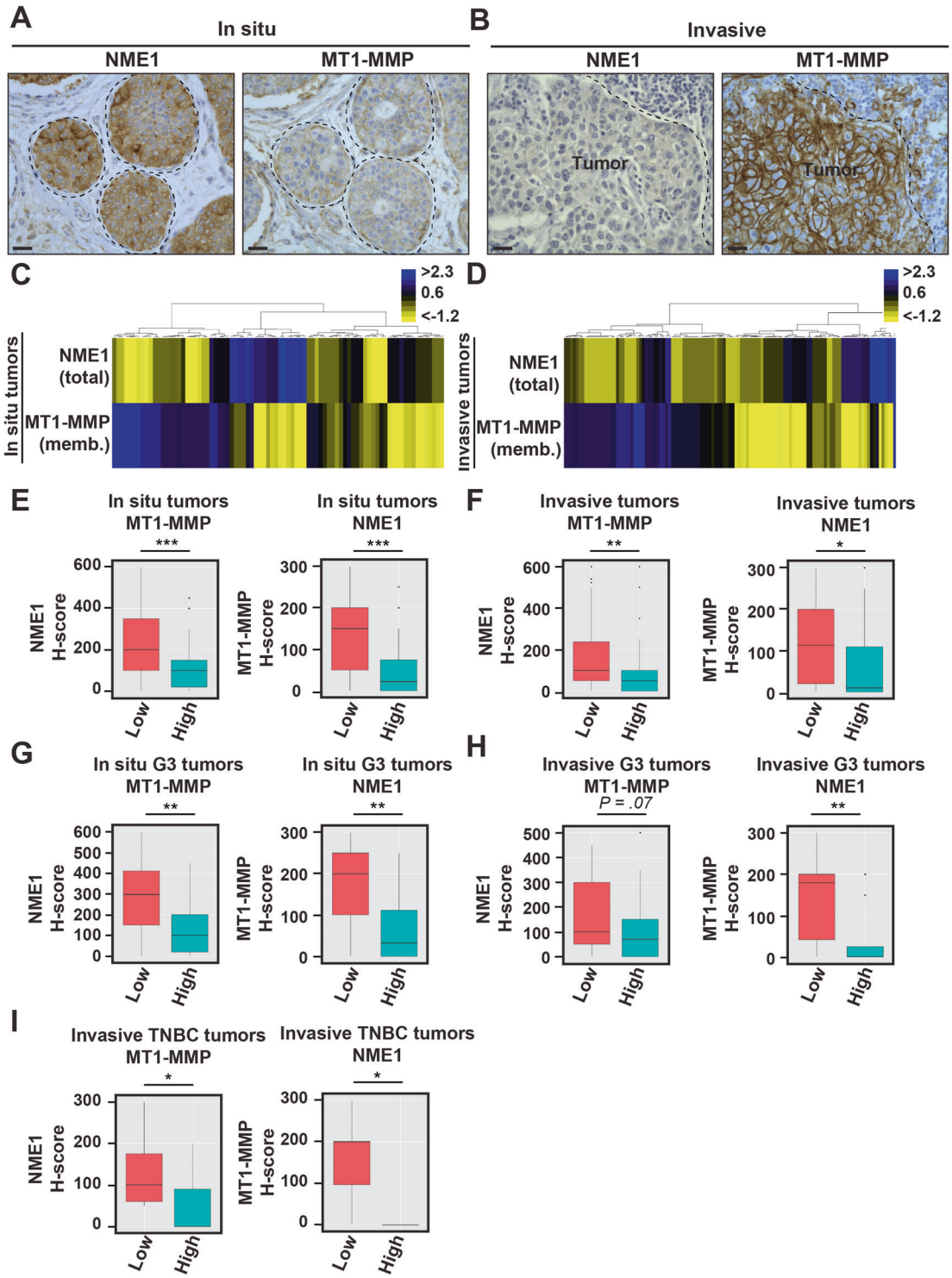

Fig. 2 Anti-correlation of NME1 and MT1-MMP cell surface levels in human breast tumors. A, **B** Representative immunostaining of NME1 and MT1-MMP on serial sections of synchronous in situ (**A**) and invasive (**B**) components of human breast carcinoma (case #1). Scale bar, 25 µm. **C**, **D** Unsupervised hierarchical clustering based on total NME1 and plasma membrane MT1-MMP expression levels in the in situ (**C**) and invasive (**D**) breast carcinoma samples. Data are shown in a table format with the vertical axis listing the biopsies. A color scale, which represents the relative staining patterns of each sample, is displayed at the top right corner. **E**, **F** Left, box-plots of NME1 protein levels (H-score) depending on membranous MT1-MMP H-score variable discretized as low and high expression from in situ (**E**) and invasive components (**F**) of the cohort of human breast tumors. Right, box-plots of membranous expression of MT1-MMP (H-score) depending on NME1 H-score variable discretized as low and high levels in in situ (**E**) and invasive components (**F**) of the human breast tumor cohort. ***$P < 0.001$; **$P < 0.01$; *$P < 0.05$. **G**, **H** Box-plots of NME1 (left) or membranous MT1-MMP levels (right) depending on the reciprocal marker segregated as low and high expression from in situ (**G**) or invasive components (**H**) of higher histological grade III (G3) breast tumors. **$P < 0.01$. **I** Box-plots of NME1 (left) or membranous MT1-MMP levels (right) depending on the reciprocal marker segregated as low and high expression from invasive TNBC tumors. *$P < 0.05$.

high histological grade III as compared to lower-grade tumors (Fig. 2G, H) and in invasive TNBC tumors (Fig. 2I). All together, our data uncovered a biphasic NME1 alteration in breast cancer with a characteristic up-regulation in DCIS lesions and a robust down-modulation at the onset of the invasive switch and in invasive lesions. Down-regulation of NME1 correlated with the up-regulation of the pro-invasive, pro-metastatic surface MT1-MMP in IBCs.

Acceleration of the invasive switch by loss of NME1 in the intraductal xenograft model

Intra-nipple injection of human breast carcinoma MCF10DCIS.com cells in the mammary glands of SCID mice generate intraductal tumors that recapitulate the DCIS-to-IBC transition [20, 23]. Using this model, we reported that loss of MT1-MMP function impaired the invasive switch [11]. The consequences of the CRISPR/Cas9-mediated knockout of NME1 or NME2 were investigated using the intraductal xenograft model (Fig. 3A and Supplementary Fig. S9). Immunoblotting analysis showed that the knockout of NME1 did not affect NME2 levels and reciprocally (Fig. 3A). In addition, immunohistochemistry staining confirmed the loss of NME1 expression in tumor xenografts generated from NME1 knockout cells (Fig. 3E, lower panel KO NME1#A). At an early time-point after intraductal injection (i.e., 4 weeks), the tumor foci generated by control MCF10DCIS.com (NT) cells were all scored in situ based on histological staining of whole-mount and tissue-sections (Fig. 3B, D). Similarly, NME2 KO cells gave rise mostly to in situ tumors, with a very small subset of tumor foci (2–3%) having invasive features (Fig. 3B, D). In contrast, intraductal injection of NME1 KO cells generated up-to 20–40% of invasive tumors (Fig. 3B, D). Some size differences were also found with larger tumors obtained upon injection of NME2 KO cells (Fig. 3C, D), which correlated with higher percentage of PCNA-positive cells in NME2-KO tumor xenografts as compared to NT or NME1-KO tumors (Supplementary Fig. S10). Therefore, overgrowth of NME2-negative tumors was related to an increase in the proliferation rate but not to the invasive status.

Strikingly, at later time-point (i.e. 7 weeks after injection), immunostaining revealed that invasive tumor xenografts obtained upon injection of control MCF10DCIS.com cells expressed low NME1 levels, in contrast to in situ tumors that were frankly positive (Fig. 3E). In addition, NME1 knockout correlated with a strong membranous MT1-MMP expression in carcinoma cells that increased in IBC vs. DCIS tumors (Fig. 3F). Therefore, the invasive switch in xenograft tumors recapitulated the main features described in human breast tumors. Collectively, these data indicated that the loss of NME1, but not of NME2, accelerated the invasive switch of breast tumors in the intraductal xenograft assay, possibly in relation with increased plasma membrane MT1-MMP levels. Thus, loss of NME1 in breast carcinoma cells is a key emerging feature of the in situ-to-invasive breast carcinoma transition.

NME1 controls the endocytic clearance and surface levels of MT1-MMP

In order to explore the mechanism underlying the enhancement of breast tumor invasion by NME1 down-modulation, the cellular distribution of NME1 was examined. In agreement with the membranous NME1 staining in IHC analyses (see above), NME1 was recovered in the dynamin-2-positive membrane fraction also enriched for MT1-MMP (Fig. 4A). Some association of NME1 with the cytosolic fraction was also detected (Fig. 4A). Furthermore, we found that NME1 as well as MT1-MMP, were enriched in a clathrin-coated vesicle fraction positive for clathrin heavy chain and in the α-adaptin subunit of the clathrin adaptor complex, AP-2 (Fig. 4B).

Proximity ligation assay (PLA) confirmed a close proximity of NME1 with dynamin-2 and α-adaptin [8] (Fig. 4C). In addition, we detected a close proximity between FLAG-tagged MT1-MMP and NME1 and dynamin-2 (Fig. 4C). Omission of any one of the primary antibodies abolished PLA signal (Fig. 4C). Therefore, our data identified a close proximity between NME1, α-adaptin, dynamin-2 and MT1-MMP in the clathrin-mediated endocytic pathway in agreement with previous findings implicating clathrin-mediated endocytosis in the internalization of MT1-MMP [16, 17, 24]. Furthermore, NME1 and MT1-MMP could be co-immunoprecipitated, and co-immunoprecipitation was abolished by NME1 knockout demonstrating specificity (Fig. 4D, E). Moreover, we found a direct interaction between recombinant NME1 and the carboxy-terminal tail of MT1-MMP fused with GST (Fig. 4F). In addition, NME1 and dynamin-2 were co-immunoprecipitated under similar conditions (Fig. 4G, H). All together, these data indicated that NME1 interacted with MT1-MMP and dynamin-2 in clathrin-coated pits.

We previously identified NME1 as an enhancer of dynamin GTPase-mediated endocytosis by providing GTP supply for dynamin's proper function in vesicle sission [8]. Therefore, we investigated the impact of genetically modified NME1 levels on the rate of MT1-MMP internalization in human breast cancer cell lines. Overexpression of NME1 in MDA-MB-435 and MDA-MB-231 cells significantly increased MT1-MMP endocytosis (Fig. 5A, B, G, H), whereas silencing of NME1 in MCF10DCIS.com or MDA-MB-231 cells significantly decreased MT1-MMP uptake (Fig. 5C, E, I, J).

Surface-exposed MT1-MMP results from a balance of endocytic and exocytic events, and is responsible for pericellular degradation of ECM components by carcinoma cells [15, 18, 19]. Immunoblot analysis in breast cancer cell

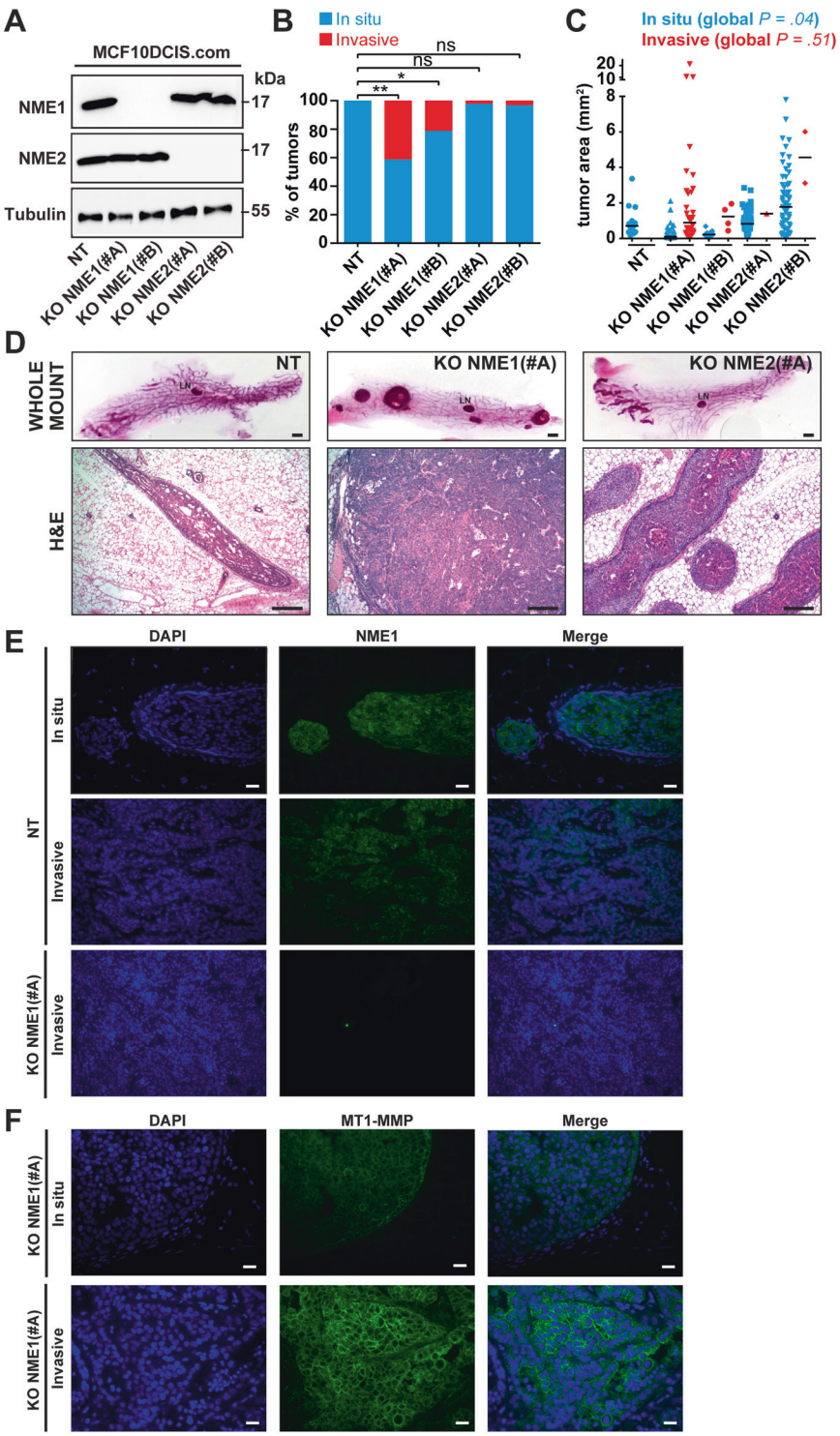

Fig. 3 Loss of NME1 function promotes the in situ-to-invasive breast tumor transition. **A** Lysates of MCF10DCIS.com clones knockout for NME1 or NME2, or control non-KO cells (NT) were analyzed by immunoblotting with the indicated antibodies. Alpha-tubulin was used as a loading control. Molecular weights are in kDa. **B** Phenotypic analysis of intraductal xenograft tumors of MCF10DCIS.com cell clones ablated for NME1 or NME2 measured 4 weeks post-intraductal injection (p.i.i.) based on whole-mount staining of the mammary glands. $^{**}P < 0.01$; $^{*}P < 0.05$; *ns* not significant. **C** Tumor area of intraductal xenograft individual tumors of NT (wild type NME1 and NME2), KO NME1, or KO NME2 MCF10DCIS.com cells 4 weeks p.i.i. after phenotypic classification into in situ or invasive status. **D** Whole-mount carmine (upper row) and H&E staining (lower row) of nipple-injected glands 4 weeks after injection of the indicated MCF10DCIS.com cell populations. Scale bars, 1 mm (whole-mount carmine), 50 µm (H&E). **E** DAPI (blue) and NME1 (green) immunofluorescence staining of sections of in situ (upper row) or invasive (lower row) intraductal tumor xenografts of control NT MCF10DCIS.com cells 4 weeks or 7 weeks after intra-nipple injection, respectively. Scale bar, 40 µm. **F** DAPI (blue) and MT1-MMP (green) immunofluorescence staining of intraductal tumor xenografts of MCF10DCIS.com cells knockout for NME1 at the in situ (upper row) or invasive (lower row) stage. Scale bar, 20 µm.

lines with genetically-modified NME1 or NME2 levels revealed no gross alteration of total MT1-MMP levels (Fig. 5A–F). Surface MT1-MMP levels were analyzed using a validated flow cytometry assay (Supplementary Fig. S11). Overexpression of NME1 in MDA-MB-435 or MDA-MB-231 cells resulted in a strong reduction of surface MT1-MMP levels (Fig. 5K, L). In reciprocal experiments, loss of NME1 function in MCF10DCIS.com cells resulted in a ~2-fold increase in MT1-MMP surface expression, while loss of NME2 had no such effect (Fig. 5C, D, F, M, N). Collectively, these data indicate that metastasis-suppressor NME1, but not NME2, controls the endocytic clearance and surface exposure of MT1-MMP in various breast cancer cell lines.

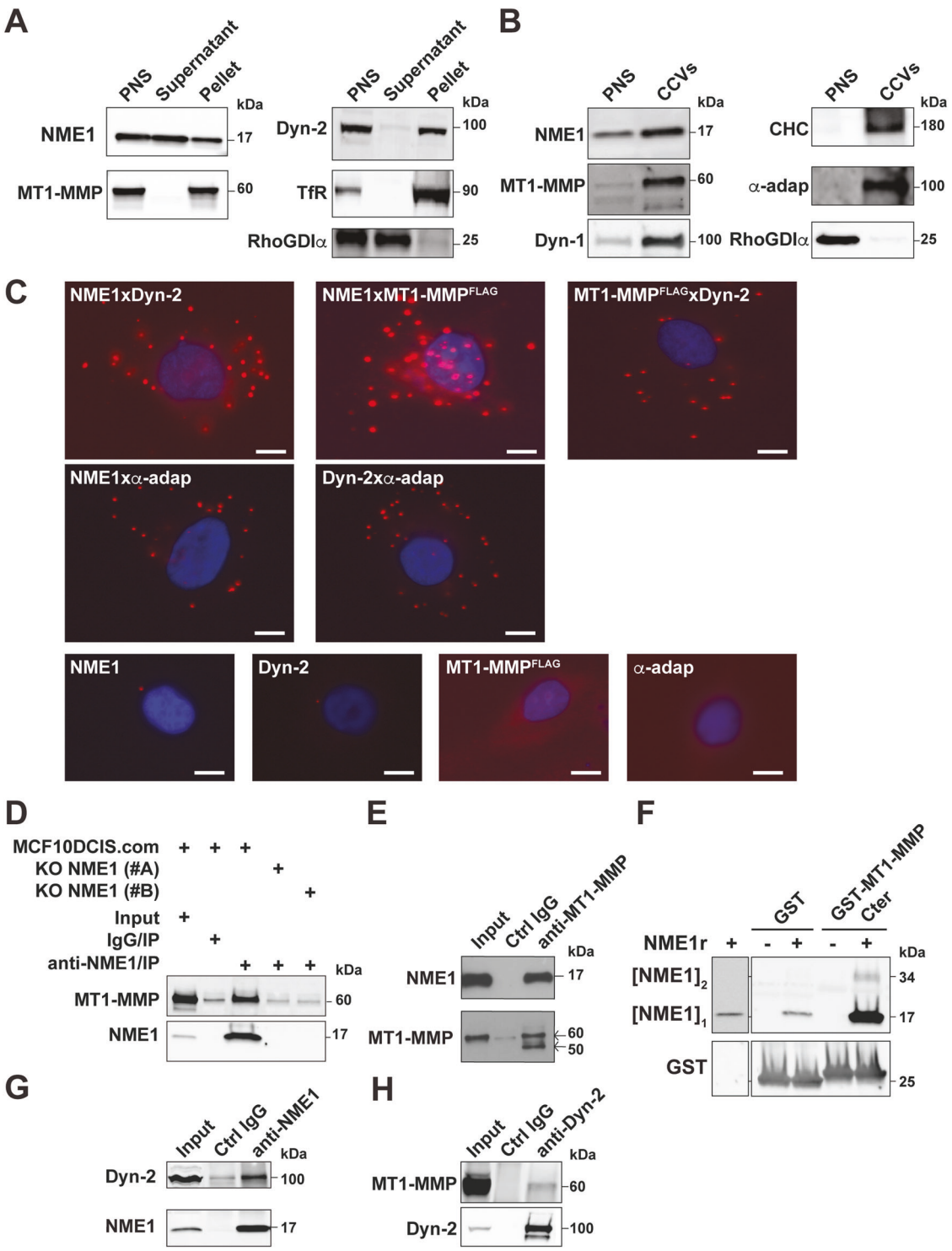

NME1 regulates MT1-MMP-dependent pericellular collagenolysis and invasion

We assessed the contribution of NME1 to the capacity of tumor cells to remodel and invade through matrix constructs consisting either of Matrigel, with a composition similar to the basement membrane, or type I collagen, the main component of the interstitial tissue. While, control and NME2-KO MCF10DCIS.com cells grew as compact spheroids in Matrigel, spheroids of cells KO for NME1 formed invasive outgrowths (Fig. 6A). Induction of an invasive program by loss of NME1 was similarly observed

◀ **Fig. 4 NME1 interacts with MT1-MMP and dynamin-2 in clathrin-coated vesicles. A** After homogenization, a post-nuclear supernatant (PNS) of MCF10DCIS.com cells was ultracentrifuged to produce soluble (Supernatant) and membrane (Pellet) fractions. Proteins corresponding to equivalent cell-number were loaded in each lane and analyzed by immunoblotting with the indicated antibodies. The transferrin receptor (TfR) was recovered in the membrane pellet fraction, while cytosolic RhoGDIα was enriched in the supernatant. Dyn-2, dynamin-2. **B** PNS and clathrin-coated vesicle (CCV) fractions (10 µg) isolated from porcine brain were analyzed by immunoblotting with the indicated antibodies. Data are representative of two independent fractionation experiments. CHC, clathrin heavy chain, α-adap, α-adaptin, Dyn-1, dynamin-1. **C** Proximity-Ligation Assay (PLA) in MCF10DCIS.com cells using the indicated antibody combinations. Lower row, background PLA signal in the presence of single primary antibody. Scale bar, 5 µm. **D** Lysates of MCF10DCIS.com cells or cells knocked out for NME1 (clones #A and #B) were immunoprecipitated with NME1 antibodies or control IgGs followed by immunoblotting analysis with MT1-MMP antibodies. 1% of total lysate was loaded as a control (input). **E** In reciprocal experiments, lysates were immunoprecipitated with MT1-MMP antibodies followed by immunoblotting analysis with NME1 antibodies. 1% of total lysate was loaded as a control (input). **F** Direct interaction between purified recombinant NME1 (NME1r) and the carboxy-terminal tail of MT1-MMP fused with GST (GST-MT1-MMP-Cter). GST is used as a control. Proteins were analyzed by immunoblotting with NME1 or GST antibodies as indicated. $[NME1]_1$, monomer; $[NME1]_2$, denaturation-resistant dimer. Lane 1 is a longer exposure of the NME1 immunoblot. **G**, **H** MCF10DCIS.com cell lysates were immunoprecipitated with NME1 (G) or dynamin-2 (H) antibodies and bound proteins were analyzed by immunoblotting with dynamin-2 or MT1-MMP antibodies as indicated. 1% of total lysate was loaded as a control (input).

in cells embedded in the 3D type I collagen network, and was abolished in the presence of GM6001, a general MMP inhibitor, or upon silencing of MT1-MMP indicating that the invasion program induced by NME1 loss-of-function required MT1-MMP activity (Fig. 6B, C and Supplementary Fig. S12A).

Finally, we investigated the consequences of the modulation of NME1/NME2 levels on the ability of tumor cells to proteolytically cleave the surrounding type I collagen fibers. We used the Col1-$^{3/4}$C mAb, which recognizes MMP-cleaved type I collagen molecules [25, 26]. Silencing of MT1-MMP in MCF10DCIS.com cells abolished pericellular collagenolysis indicating that type I collagen degradation strongly relied on MT1-MMP activity (Fig. 6D, E). Knockdown of NME1 led to a 1.5-2-fold increase in pericellular collagenolysis, in contrast to NME2 silencing that did not affect collagenolysis (Fig. 6D–F and Supplementary Fig. 12B). Moreover, silencing of MT1-MMP abolished the induction of pericellular collagenolysis upon NME1 loss of function (Fig. 6F). Collectively, these data indicate that MT1-MMP mediates both an increase in invasion and collagenolysis in breast cancer cells with reduced NME1 activity.

The regulation of collagenolysis by NME1 could be generalized by overexpression in MDA-MB-435 cells that express barely detectable level of NME1 (Fig. 5A), resulting in a strong 80% reduction of collagenolysis (Fig. 6G, H). Thus, we conclude that NME1, not NME2, is an essential element of the pericellular matrix proteolysis and invasion programs of breast tumor cells by controlling the clearance and surface expression of MT1-MMP in breast carcinoma cells (see Model in Fig. 6I).

Discussion

Down-modulation of NME1 NDPK expression is known to correlate with metastatic dissemination and worse prognosis in several cancer types, including breast cancers [27–29]. However, NME1's implication in local invasion at the in situ-to-invasive breast carcinoma transition has been overlooked, and the mechanisms underlying metastasis suppression by NME1 remained largely unknown.

Our IHC analysis of breast tumor specimens based on highly discriminating antibodies revealed an up-regulation of NME1 levels in carcinoma cells in DCIS tumors as compared to surrounding non-malignant tissues, whereas NME1 levels were significantly reduced in synchronous invasive tumor foci and in microinvasive carcinoma buds extending beyond the ruptured basement membrane. Thus, we propose NME1 as a potential marker to predict in situ tumors with high risk to progress into invasive breast carcinomatous lesions, which remains a critical issue in breast cancer management [30]. Supporting our conclusion, NME1 is also reduced or absent at the invasive front of human hepatocellular carcinoma and colon cancers, as compared to its strong expression in the tumor central area [31]. Taken together, these data suggest that the reduction of NME1 expression during the progression to invasive disease is a generic feature of epithelial tumor progression.

We found a strong anti-correlation of NME1 and cortical MT1-MMP expression in invasive breast carcinomatous lesions. Anti-correlation of NME1/MT1-MMP levels was confirmed in RNAseq data in invasive breast carcinoma (TCGA, not shown). This anti-correlation was additionally observed in carcinomas of various origin including colon, endometrial, ovarian, prostate, and head and neck squamous carcinoma tumors (TCGA, not shown), indicating that negative control of MT1-MMP activity in matrix remodeling is a generic trait of the metastasis-suppressive function of NME1, which is lost upon repression of NME1 expression during cancer progression. In addition, based on the intraductal xenograft model, [20], we have shown that down-modulation of NME1 accelerated the invasive transition in breast carcinoma. Together with the potent inhibition of the invasive switch caused by the loss of MT1-MMP in the intraductal model [11], these convergent findings suggested that the loss of NME1 function in breast tumor

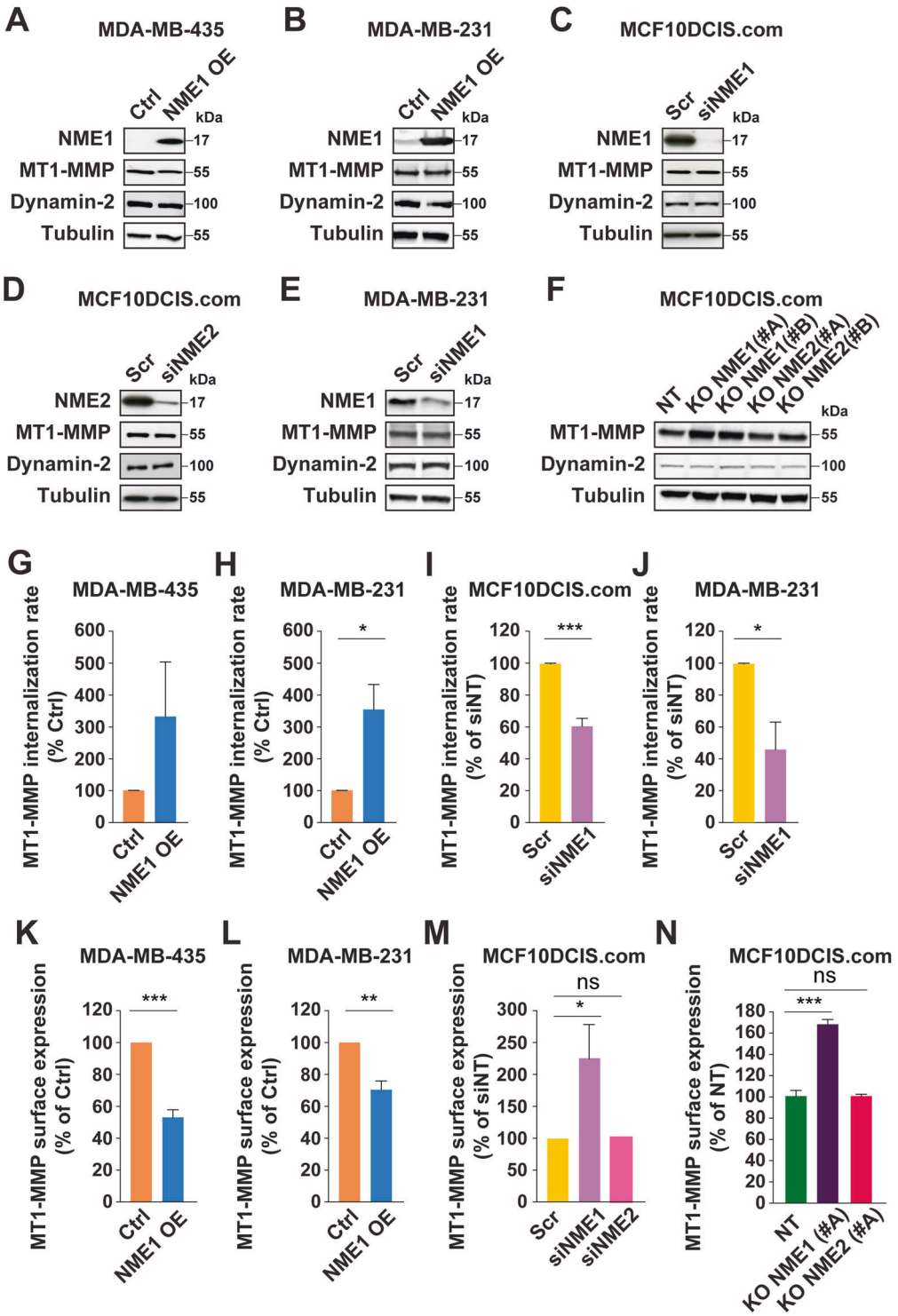

Fig. 5 Modulation of NME1 levels impacts the endocytosis rate and surface levels of MT1-MMP in breast cancer cells. A, **B** Lysates of MDA-MB-435 and MDA-MB-231 cells overexpressing NME1 (NME1 OE) were analyzed by immunoblotting with the indicated antibodies. **C**, **D**, **E** MCF10DCIS.com or MDA-MB-231 cells were silenced for NME1 or NME2 by siRNA treatment and lysates were analyzed by immunoblotting with the indicated antibodies. **F** Lysates of MCF10DCIS.com cells knockout for NME1 or NME2, or control non-KO cells were analyzed by immunoblotting with the indicated antibodies. **G**, **H**, **I**, **J** NME1 levels were modulated by overexpression (**G**, **H**) or silencing (**I**, **J**) in the indicated breast cancer cell lines, and MT1-MMP endocytosis rate was measured using a cell-surface biotinylation assay after 60 min incubation at 37 °C. Three independent experiments were performed. Error bars are the standard error of the mean (SEM). $***P < 0.001$; $*P < 0.05$. For (**G**), although not statistically significant, overexpression of NME1 in MDA-MB-435 cells clearly tended to increase MT1-MMP endocytosis (6.7-, 2.1-, and 1.2-fold increase for each of the three independent experiments). **K**, **L**, **M**, **N** NME1 levels were modulated in different breast cancer cell lines as indicated, and surface MT1-MMP levels were analyzed by FACS. Four independent experiments were performed for (**K**, **L**, **M**). Three independent experiments were performed for (**N**). Error bars are the standard error of the mean (SEM). $***P < 0.001$; $**P < 0.01$; $*P < 0.05$; *ns* not significant.

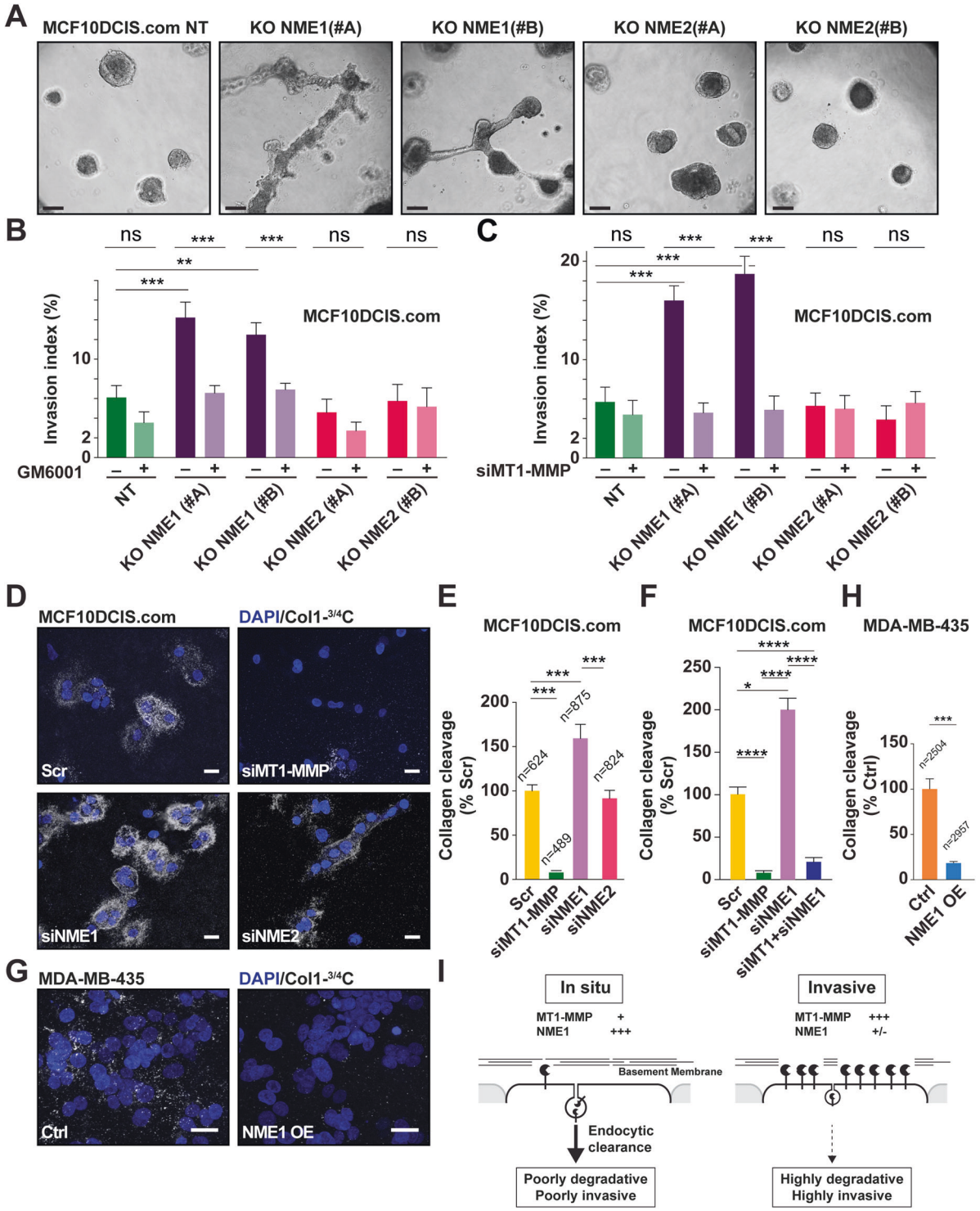

epithelial cells could unleash MT1-MMP proinvasive activity. Complex regulatory networks based on transcriptional regulators including p63 and AIB1/YAP have been identified as drivers of malignant progression, invasion and proliferation during breast cancer progression [2, 11, 32, 33]. Whether these different regulatory circuits play a role in the biphasic NME1 expression profile and MT1-MMP up-regulation during breast cancer progression will be interesting to examine in future studies.

In order to work efficiently, dynamin, which has a low affinity for GTP and a high intrinsic GTPase activity, needs to be permanently reloaded with GTP, which is provided by NME1 and NME2 NDPKs [8]. In addition, NME1 has been proposed to facilitate the oligomerization and GTPase

◀ **Fig. 6 NME1 controls invasive and matrix-degradative potential of breast cancer cells through MT1-MMP activity. A** Independent clones of MCF10DCIS.com cells knockout for NME1 or NME2 or non-KO control cells (NT) were embedded in Matrigel as a single cell suspension followed by a 7-d culture and imaged by differential interference contrast microscopy. Scale bar, 50 µm. **B** MCF10DCIS.com cells knockout for NME1 or NME2 were seeded on a type I collagen gel and cultured for 24 h in the absence or the presence of MMP inhibitor, GM6001. Invasive index represents the percentage of cells invading the gel divided by the total number of cells from two independent experiments. Error bars are the standard error of the mean (SEM). $***P < 0.001$; $**P < 0.01$; *ns* not significant. **C** MCF10DCIS.com cells knockout for NME1 or NME2 were silenced for MT1-MMP expression by siRNA treatment and assayed for type I collagen invasion as in panel (**B**). Two independent experiments were performed. Error bars are the standard error of the mean (SEM). $***P < 0.001$; *ns* not significant. **D** MCF10DCIS.com cells treated with the indicated siRNAs were embedded in collagen I and stained for cleaved collagen I with Col1-$^{3/4}$C pAb (white). DAPI-stained nuclei are shown in blue. Scale bar, 20 µm. **E** Pericellular collagenolysis was detected using Col1-$^{3/4}$C pAb as in panel (**D**). Values are mean normalized degradation index ± SEM. *n* number of cells analyzed for each cell population from three independent experiments. $***P < 0.001$. **F** MCF10DCIS.com cells treated with the indicated siRNAs were embedded in collagen I and pericellular collagenolysis was scored as in panel (**D**, **E**). **G**, **H** MDA-MB-435 cells transfected with the empty control vector (Ctrl) or overexpressing NME1 (NME1 OE) were embedded in type I collagen and pericellular collagenolysis was detected and scored. Scale bar, 20 µm. **I** Scheme recapitulating the function of NME1 in promoting the endocytic clearance of MT1-MMP in relation with the invasive switch of breast cancer.

activity of dynamin [34]. Both GTP channeling and stimulation of dynamin oligomerization by NME1/2 contribute to the stimulation of dynamin function in vesicle scission. Endocytosis is a major mean by which cells regulate MT1-MMP cell surface levels, which directly impinge on pericellular ECM degradation [15, 18]. We show here that NME1 interacts directly with the cytosolic domain of trans-membrane MT1-MMP and with ubiquitously-expressed dynamin-2 in clathrin-coated pits, and that the reduction of NME1 function impairs both MT1-MMP endocytosis in relation with an increase in surface exposure, and consequent enhancement of the degradation of the pericellular ECM mediated by MT1-MMP (see Model in Fig. 6I). These data are in agreement with a marked defect in internalization and strong enhancement of collagenolysis reported for a tail-deleted MT1-MMP construct [24]. Noteacibly, we and others reported that, besides its role in endocytosis at the plasma membrane, dynamin-2 also localizes to (MT1-MMP-positive) endolysosomal compartments where it is required for the recycling of MT1-MMP and co-trafficking cargoes, such as flotillins, from endolysosomes back to the surface [35–38]. Inhibition or silencing of dynamin-2 was shown to impair invadopodia activity and matrix degradation [36], opposite of what is seen upon NME1 inhibition. Furthermore, dynamin-2 has been shown to act as a positive regulatory factor of matrix degradation and metastasis, in relation with its role in actin cytoskeleton organization and actin dynamics at invadopodia and in podosomes [39–42]. Therefore, the regulation of ECM degradation by dynamin-2 is complex and not limited to dynamin-2's role in MT1-MMP surface clearance through clathrin-mediated endocytosis.

A further layer of complexity is that the modulation of MT1-MMP surface levels, in relation with changes in NME1 expression such as the one we found in breast cancers, may affect other MMPs' function and membrane proteins that are known to be shedded by MT1-MMP, such as integrins or CD44, also with consequence for invasion and metastasis [15]. In preliminary analyses, we found that similar to NME1, NME2 can be detected in membrane and cytosolic fractions prepared from MCF10DCIS.com cells, and is enriched in a clathrin-coated vesicle fraction (Supplementary Fig. S13A, B). This distribution is expected given that NME2 interacts and forms catalytically active hetero-hexamers with NME1 [4, 8]. In addition, NME2 could be co-immunoprecipitated with MT1-MMP (Supplementary Fig. S13C). At this stage, information regarding the relative expression of NME1 and NME2 and stoichiometry of NME1/NME2 hetero-hexamers in different breast cancer cells is missing. In addition, we do not know whether co-immunoprecipitation of NME2 with MT1-MMP relies on a direct interaction between these two proteins or is mediated by another protein that could be NME1. Yet, our data clearly support the conclusion that NME2 knockout, that does not affect NME1 expression levels (Fig. 3A), does not impair the invasive and collagenolysis capacity of MCF10DCIS.com cells, in sharp contrast with NME1 loss of function (Fig. 6A–E).

Here, we report a role for NME1 on the acquisition of invasive traits in breast epithelial cancer cells. As the loss of NME1 may be a prerequisite for the induction of invasive features in patients with DCIS, we anticipate that its clinical management may prevent or delay the invasive switch of breast cancers. In this regard, NME1 expression in breast cancer as well as other carcinomas might be used as a prognostic factor for monitoring progression to invasive states. Finally, while therapeutic efforts aimed at targeting a proteolytic enzyme that undergoes continuous recycling at the cell surface might prove problematic, therapies directed at increasing NME1 expression might prove effective at preventing or interfering with the tissue-invasive behavior of aggressive breast cancers.

Acknowledgements The authors acknowledge the Breast Cancer Study Group and the Incentive and Cooperative Research Program "Breast cancer: Cell Invasion and Motility" and patients of Institut Curie for the breast tumor samples, Drs. C. Tomasetto, P. De camilli, P. S. Steeg and E. Smythe for kindly providing reagents, cell lines and samples for this study, the Nikon Imaging Centre @ Institut Curie-CNRS and Cell and Tissue Imaging Facility of Institut Curie, member

of the France Bio Imaging national research infrastructure (ANR-10-INBS-04) for help with image acquisition, F. Guillonneau from the Proteomic Facility 3P5, Paris-Descartes University for MALDI-MS analysis, Sandra Antoine from Institut Curie for help with the collagenolysis assay, and C. Kikuti from Institut Curie for help with SEC-MALS analysis. This work was supported by grants from the NIH/NCI to S.J.W and X.Y.L. (R01 CA071699) as well as the Breast Cancer Research Foundation and the Margolies Family Discovery Fund for Cancer Research to S.J.W and X.Y.L. Additional support was provided by the University of Michigan Rogel Cancer Center Support Grant (P30 CA046592). Funding for this work was provided by Fondation ARC pour la Recherche sur le Cancer (PGA1 RF20170205408) and Fondation Ruban Rose (Prix Avenir 2018) to PC, the Groupement des Entreprises Françaises contre le Cancer (GEFLUC), Cancéropole-Ile de France (n° 2015-1-EMERG-25-INSERM 6-1) and PLAN CANCER (Project C19048DS) to MB.

Author contributions PC and MB designed research. CL, LF, MI, OP, XYL, HBK, SV, CC, ODW, IB, and MB performed research. CL, LF, MI, OP, XYL, HBK, FR, SV, CC, ODW, IB, MLL, AME, AH, AVS, SJW, and MB analyzed data. PC and MB wrote the paper.

Compliance with ethical standards

Conflict of interest The authors declare no competing interests.

Publisher's note Springer Nature remains neutral with regard to jurisdictional claims in published maps and institutional affiliations.

References

1. Cowell CF, Weigelt B, Sakr RA, Ng CK, Hicks J, King TA, et al. Progression from ductal carcinoma in situ to invasive breast cancer: revisited. Mol Oncol. 2013;7:859–69.
2. Lee S, Stewart S, Nagtegaal I, Luo J, Wu Y, Colditz G, et al. Differentially expressed genes regulating the progression of ductal carcinoma in situ to invasive breast cancer. Cancer Res. 2012;72:4574–86.
3. Casasent AK, Edgerton M, Navin NE. Genome evolution in ductal carcinoma in situ: invasion of the clones. J Pathol. 2017;241:208–18.
4. Boissan M, Schlattner U, Lacombe ML. The NDPK/NME superfamily: state of the art. Lab Invest. 2018;98:164–74.
5. Steeg PS, Bevilacqua G, Kopper L, Thorgeirsson UP, Talmadge JE, Liotta LA, et al. Evidence for a novel gene associated with low tumor metastatic potential. J Natl Cancer Inst. 1988;80:200–4.
6. Ouatas T, Salerno M, Palmieri D, Steeg PS. Basic and translational advances in cancer metastasis: Nm23. J Bioenerg Biomembr. 2003;35:73–9.
7. Dammai V, Adryan B, Lavenburg KR, Hsu T. Drosophila awd, the homolog of human nm23, regulates FGF receptor levels and functions synergistically with shi/dynamin during tracheal development. Genes Dev. 2003;17:2812–24.
8. Boissan M, Montagnac G, Shen Q, Griparic L, Guitton J, Romao M, et al. Membrane trafficking. Nucleoside diphosphate kinases fuel dynamin superfamily proteins with GTP for membrane remodeling. Science. 2014;344:1510–5.
9. Zala D, Schlattner U, Desvignes T, Bobe J, Roux A, Chavrier P, et al. The advantage of channeling nucleotides for very processive functions. F1000Res. 2017;6:724.
10. Szabova L, Chrysovergis K, Yamada SS, Holmbeck K. MT1-MMP is required for efficient tumor dissemination in experimental metastatic disease. Oncogene. 2008;27:3274–81.
11. Lodillinsky C, Infante E, Guichard A, Chaligne R, Fuhrmann L, Cyrta J, et al. p63/MT1-MMP axis is required for in situ to invasive transition in basal-like breast cancer. Oncogene. 2016;35:344–57.
12. Perentes JY, Kirkpatrick ND, Nagano S, Smith EY, Shaver CM, Sgroi D, et al. Cancer cell-associated MT1-MMP promotes blood vessel invasion and distant metastasis in triple-negative mammary tumors. Cancer Res. 2011;71:4527–38.
13. Feinberg TY, Zheng H, Liu R, Wicha MS, Yu SM, Weiss SJ. Divergent matrix-remodeling strategies distinguish developmental from neoplastic mammary epithelial cell invasion programs. Dev Cell. 2018;47:145–60.
14. Rowe RG, Weiss SJ. Breaching the basement membrane: who, when and how? Trends Cell Biol. 2008;18:560–74.
15. Gifford V, Itoh Y. MT1-MMP-dependent cell migration: proteolytic and non-proteolytic mechanisms. Biochem Soc Trans. 2019;47:811–26.
16. Uekita T, Itoh Y, Yana I, Ohno H, Seiki M. Cytoplasmic tail-dependent internalization of membrane-type 1 matrix metalloproteinase is important for its invasion-promoting activity. J Cell Biol. 2001;155:1345–56.
17. Jiang A, Lehti K, Wang X, Weiss SJ, Keski-Oja J, Pei D. Regulation of membrane-type matrix metalloproteinase 1 activity by dynamin-mediated endocytosis. Proc Natl Acad Sci U.S.A. 2001;98:13693–8.
18. Poincloux R, Lizarraga F, Chavrier P. Matrix invasion by tumour cells: a focus on MT1-MMP trafficking to invadopodia. J Cell Sci. 2009;122:3015–24.
19. Castro-Castro A, Marchesin V, Monteiro P, Lodillinsky C, Rosse C, Chavrier P. Cellular and molecular mechanisms of MT1-MMP-dependent cancer cell invasion. Annu Rev Cell Dev Biol. 2016;32:555–76.
20. Behbod F, Kittrell FS, LaMarca H, Edwards D, Kerbawy S, Heestand JC, et al. An intraductal human-in-mouse transplantation model mimics the subtypes of ductal carcinoma in situ. Breast Cancer Res. 2009;11:R66.
21. de Mascarel I, MacGrogan G, Mathoulin-Pelissier S, Soubeyran I, Picot V, Coindre JM. Breast ductal carcinoma in situ with microinvasion: a definition supported by a long-term study of 1248 serially sectioned ductal carcinomas. Cancer. 2002;94:2134–42.
22. Sopik V, Sun P, Narod SA. Impact of microinvasion on breast cancer mortality in women with ductal carcinoma in situ. Breast Cancer Res Treat. 2018;167:787–95.
23. Miller FR, Santner SJ, Tait L, Dawson PJ. MCF10DCIS.com xenograft model of human comedo ductal carcinoma in situ. J Natl Cancer Inst. 2000;92:1185–6.
24. Li XY, Ota I, Yana I, Sabeh F, Weiss SJ. Molecular dissection of the structural machinery underlying the tissue-invasive activity of membrane type-1 matrix metalloproteinase. Mol Biol Cell. 2008;19:3221–33.

25. Wolf K, Wu YI, Liu Y, Geiger J, Tam E, Overall C, et al. Multi-step pericellular proteolysis controls the transition from individual to collective cancer cell invasion. Nat Cell Biol. 2007;9:893–904.
26. Monteiro P, Rosse C, Castro-Castro A, Irondelle M, Lagoutte E, Paul-Gilloteaux P, et al. Endosomal WASH and exocyst complexes control exocytosis of MT1-MMP at invadopodia. J Cell Biol. 2013;203:1063–79.
27. Boissan M, Wendum D, Arnaud-Dabernat S, Munier A, Debray M, Lascu I, et al. Increased lung metastasis in transgenic NM23-Null/SV40 mice with hepatocellular carcinoma. J Natl Cancer Inst. 2005;97:836–45.
28. Marino N, Nakayama J, Collins JW, Steeg PS. Insights into the biology and prevention of tumor metastasis provided by the Nm23 metastasis suppressor gene. Cancer Metastasis Rev. 2012;31:593–603.
29. Tan CY, Chang CL. NDPKA is not just a metastasis suppressor—be aware of its metastasis-promoting role in neuroblastoma. Lab Invest. 2018;98:219–27.
30. van Seijen M, Lips EH, Thompson AM, Nik-Zainal S, Futreal A, Hwang ES, et al. Ductal carcinoma in situ: to treat or not to treat, that is the question. Br J Cancer. 2019;121:285–92.
31. Boissan M, De Wever O, Lizarraga F, Wendum D, Poincloux R, Chignard N, et al. Implication of metastasis suppressor NM23-H1 in maintaining adherens junctions and limiting the invasive potential of human cancer cells. Cancer Res. 2010;70:7710–22.
32. Hu M, Yao J, Carroll DK, Weremowicz S, Chen H, Carrasco D, et al. Regulation of in situ to invasive breast carcinoma transition. Cancer Cell. 2008;13:394–406.
33. Kushner MH, Ory V, Graham GT, Sharif GM, Kietzman WB, Thevissen S, et al. Loss of ANCO1 repression at AIB1/YAP targets drives breast cancer progression. EMBO Rep. 2020;21: e48741.
34. Khan I, Gril B, Steeg PS. Metastasis suppressors NME1 and NME2 promote dynamin 2 oligomerization and regulate tumor cell endocytosis, motility, and metastasis. Cancer Res. 2019;79:4689–702.
35. Nicoziani P, Vilhardt F, Llorente A, Hilout L, Courtoy PJ, Sandvig K, et al. Role for dynamin in late endosome dynamics and trafficking of the cation-independent mannose 6-phosphate receptor. Mol Biol Cell. 2000;11:481–95.
36. Rosse C, Lodillinsky C, Fuhrmann L, Nourieh M, Monteiro P, Irondelle M, et al. Control of MT1-MMP transport by atypical PKC during breast-cancer progression. Proc Natl Acad Sci U.S.A. 2014;111:E1872–9.
37. Meister M, Zuk A, Tikkanen R. Role of dynamin and clathrin in the cellular trafficking of flotillins. FEBS J. 2014;281:2956–76.
38. Planchon D, Rios Morris E, Genest M, Comunale F, Vacher S, Bieche I. et al. MT1-MMP targeting to endolysosomes is mediated by upregulation of flotillins. J Cell Sci. 2018;131:jcs218925.
39. Ochoa GC, Slepnev VI, Neff L, Ringstad N, Takei K, Daniell L, et al. A functional link between dynamin and the actin cytoskeleton at podosomes. J Cell Biol. 2000;150:377–89.
40. Baldassarre M, Pompeo A, Beznoussenko G, Castaldi C, Cortellino S, McNiven MA, et al. Dynamin participates in focal extracellular matrix degradation by invasive cells. Mol Biol Cell. 2003;14:1074–84.
41. Eppinga RD, Krueger EW, Weller SG, Zhang L, Cao H, McNiven MA. Increased expression of the large GTPase dynamin 2 potentiates metastatic migration and invasion of pancreatic ductal carcinoma. Oncogene. 2012;31:1228–41.
42. Razidlo GL, Wang Y, Chen J, Krueger EW, Billadeau DD, McNiven MA. Dynamin 2 potentiates invasive migration of pancreatic tumor cells through stabilization of the Rac1 GEF Vav1. Dev Cell. 2013;24:573–85.

Metastasis-suppressor NME1 controls the invasive switch of breast cancer by regulating MT1-MMP surface clearance

Catalina Lodillinsky[1,2], Laetitia Fuhrmann[3], Marie Irondelle[4], Olena Pylypenko[4], Xiao-Yan Li[5], Hélène Bonsang-Kitzis[6,7,¶], Fabien Reyal[6,7], Sophie Vacher[8], Claire Calmel[9], Olivier De Wever[10], Ivan Bièche[8], Marie-Lise Lacombe[9], Ana Maria Eiján[1,2], Anne Houdusse[4], Anne Vincent-Salomon[3], Stephen J. Weiss[5], Philippe Chavrier[4,‡] and Mathieu Boissan[9,11,‡,*]

‡ Philippe Chavrier and Mathieu Boissan contributed equally to the work

[1] Research Area, Instituto de Oncología Ángel H. Roffo, Universidad de Buenos Aires, Buenos Aires, Argentina

[2] Consejo Nacional de Investigaciones Científicas y Técnicas (CONICET), Buenos Aires, Argentina

[3] Institut Curie, PSL Research University, Diagnostic and Theranostic Medicine Division, Paris, France

[4] Institut Curie, PSL Research University, CNRS UMR144, Paris, France

[5] Division of Medical Genetics, Department of Internal Medicine, Life Sciences Institute, University of Michigan, Ann Arbor MI, USA

[6] Department of Surgery, Institut Curie, Paris, France

[7] Translational Research Department, RT2Lab Team, INSERM U932, Immunity and Cancer, Institut Curie, Paris, France

[8] Pharmacogenomic Unit, Institut Curie, Paris, France

[9] University Sorbonne, INSERM UMR_S 938, Saint-Antoine Research Center, CRSA, Paris, France

[10] Laboratory of Experimental Cancer Research, Cancer Research Institute Ghent (CRIG), Department of Human Structure and Repair, Ghent University, Ghent, Belgium

[11] Laboratory of Biochemistry and Hormonology, Tenon Hospital, AP-HP, Paris, France

¶ Present address: Gynecological and Breast Surgery and Cancerology Center, RAMSAY-Générale de Santé, Hôpital Privé des Peupliers, Paris, France

* Corresponding author: Mathieu Boissan, University Sorbonne, INSERM UMR_S 938, Saint-Antoine Research Center, CRSA, Paris, France. E-mail: mathieu.boissan@inserm.fr; Tel: +33 1 49 28 46 32

Supplemental experimental procedures

Cell culture

MCF10DCIS.com cell line was purchased from Asterand (Detroit, MI, USA) and maintained in advanced DMEM/F12 media supplemented with 5% horse serum and 2 mM glutamine at 37°C in 5% CO_2. MDA-MB-435 were maintained in DMEM supplemented with 10% fetal calf serum and 2 mM glutamine at 37°C in 5% CO_2. MDA-MB-231 cell line was obtained from the American Type Culture Collection (ATCC HTB-26, LGC Promochem) and maintained in L-15 culture medium with 2 mM glutamine and 15% fetal calf serum at 37°C in 1% CO_2.

DNA constructs

C-terminally FLAG-tagged MT1-MMP construct was generated by inserting primers encoding the FLAG epitope (5'-GACTACAAGGACGACGATGACAAG-3') after the COOH-terminal valine of the molecule and cloned in pCR3.1 Uni as previously described [1].

Antibodies

Highly specific NME1 and NME2 rabbit polyclonal antibodies (pAbs) were previously described [2]. Rabbit pan-NME pAb (recognizing both NME1 and NME2 isoforms) were prepared by affinity purification using purified human recombinant NME1 and NME2 proteins coupled to NHS-activated HiTrap columns [2]. Mouse NME1 (UMAB94) and NME2 (clone KM1121) monoclonal antibodies (mAbs) were purchased from OriGene (Rockville, MD) and Kamiya Biomedical Company (Seattle, WA), respectively. Rabbit dynamin-2 pAb and mouse dynamin-1 mAb were a kind gift of Dr. P. De Camilli (Yale University School of Medicine, New Haven, CT). Mouse α-adaptin

mAb (clone AC1-M11) was obtained from Abcam (Cambridge, MA, USA). Rabbit α-adaptin 1/2 (M-300) and Rho GDIα (A-20) pAbs were purchased from Santa Cruz Biotechnology (Santa Cruz, CA). Mouse MT1-MMP mAb (clone LEM-2/15.8) was purchased from Millipore (Molsheim, France) and used for western blotting, immunofluorescence and immunoprecipitation analyses. Mouse MT1-MMP mAb (clone 2D7, a kind gift from C.L. Tomasetto, IGBMC, Illkirch, France [3]), was used for flow cytometry analysis. Mouse PCNA mAb was purchased from Cell Signaling Technology (Beverly, MA). Mouse transferrin receptor mAb (clone H 68.4) was obtained from Zymed Laboratories (South San Francisco, CA). Mouse α-tubulin mAb (clone DM1A) was purchased from Thermo Fisher Scientific (St. Louis, MO).

RNA interference

All siRNA oligonucleotides were synthesized by Ambion^{R} Life Technologies (Applied Biosystems, Austin, TX). The following siRNAs were used for NME1, pooled 5'-GGAUUCCGCCUUGUUGGUC-3' and 5'-GGCUGUAGGAAAUCUAGUU-3'; NME2, pooled 5'-GGAUUGAUCAUUCUUUUAU-3' and 5'-GCCUAUGGUUUAAGCCUGA-3'; irrelevant control siRNA: 5'-GGCUGUAGAAGCUAUAGUU-3'. MCF10DCIS.com cells were transfected with 100 nM control (scrambled siRNA) or specific siRNA duplex using Lullaby reagent (OZ Biosciences, Marseille, France). Protein depletion was verified by immunoblotting analysis with specific antibodies and was maximal after 72 hrs of siRNA treatment.

CRISPR/Cas9 technology

CRISPR guides. Lentiviral plasmid guides targeting human NME1 and NME2 were generated in pLenti U6gRNA Cas9-GFP-Puro vector and were purchased from Merck-

Sigma-Aldrich as well as the non-target guide (pLenti CRISPR-NT CONTROL). Two different guides were designed (https://www.milliporesigmabioinfo.com/bioinfo_tools/) for NME1: NME1-A [#HS0000009943, target sequence GACGGGCCGAGTCATGCTCGGG] and NME1-B [#HS0000009940, target sequence GAACACTACGTTGACCTGAAGG], and for NME2: NME2-A [#HS0000056847, target sequence TCATCGCCATCAAGCCGGACGG] and NME2-B [#NME2_0_76, target sequence AAGACCGACCATTCTTCCCTGG].

Lentiviral vectors production and MCF10DCIS.com cells transduction. These steps were performed with help of the GIGA Viral vectors platform (University of Liège, Belgium). Briefly, Lenti-X 293T cells (Clontech) were co-transfected together with pLenti U6gRNA NME1-Cas9-GFP-Puro or pLenti U6gRNA NME2-Cas9-GFP-Puro or pLenti CRISPR-NT CONTROL and with pcgpV (Cell Biolabs), pRSV-Rev (Cell Biolabs) and VSV-G (Cell Biolabs) encoding vectors. Lentiviral supernatants were collected 48 to 96 hrs post-transfection, filtrated and concentrated 100x by ultracentrifugation. Lentivirus stocks were titrated with qPCR Lentivirus Titration (Titer) Kit (abm) and used to transduce cells. After 72 hrs, cells were selected with 2 µg/ml puromycin (Cayla/Invivogen). Then, cells expressing GFP were isolated and cloned by FACS on a FACSaria III 4L sorter (BD Biosciences). Each clone was tested by western blotting and immunofluorescence analysis. Clones that were negative for NME1 or NME2 expression were selected for further experiments.

Sequencing. Selected clones were analyzed by miSeq in order to confirm mutations in NME1 or NME2-coding sequences. DNA were extracted from cell pellets using Maxwell® 16 Blood DNA Purification Kit. Primers flanking the CRISPR-Cas9 target sites were designed with Primer3 based on the UCSC hg19 human reference genome. Nextera XT adapter overhangs sequences and primers sequences are in Table S1.

For all clones, amplicons were generated for the four targeted regions (NME1A, NME1B, NME2A, and NME2B) using Q5 High-Fidelity DNA Polymerase (New England Biolabs). PCR1 products were purified with Ampure beads. Illumina sequencing adapters and dual index barcodes were added to the amplicon target libraries with only 8 cycles PCR using Kapa Hifi HotStart ready mix (as described in 16s workflow Illumina guide). Different combinations of Nextera XT index were used for each sample, PCR2 products were then purified with AMpure beads, quantified with picogreen dsDNA quantitation assay and normalized at 7 ng/µl and then pooled. Before proceeding to High throughput sequencing, the final pools were quantified by qPCR (KAPA SYBR FAST kit (ABI Prism). Final libraries were spiked (8%) into a Miseq run 300 cycles v2 (Read1: 156 cy, Read2:160 cy, index1: 8cy, index2: 8cy).

Sequence analysis. Raw reads were demultiplexed and adapter-trimmed using Illumina bcl2fastq. Analysis of the sequencing data was performed using CRISPResso v1.0.2 (Ref: https://www.ncbi.nlm.nih.gov/pubmed/27404874) comparing for each amplicon of each clone, the sequencing data to the corresponding region of the UCSC hg38 reference the Human genome. Reads containing insertions and/or deletion (indel) with respect to the reference amplicon sequence were identified and considered as edited while reads only containing substitutions were conservatively considered as not edited (CRISPResso options: --ignore_substitutions and no guide provided). The region of the amplicon containing coding sequences was also provided to identify out-of-frame indels (CRISPResso -c option). Analyses performed in CRISPResso with alternative options (counting modifications in a window of 7 nucleotides around the predicted cutting site and with or without ignoring substitutions) gave similar results. Sequencing results were also checked visually in the Integrative Genome Viewer after

alignment directly to the entire UCSC hg38 Human reference genome with BWA v0.7.5a (BWA mem algorithm).

Human breast tumor samples and tissue microarray construction

Approximately one hundred sixty samples of primary breast tumors harboring synchronous DCIS and IBC, and 37 microinvasive breast carcinomas (defined as infiltrating carcinomas with one or more areas of focal invasion, none larger than 1 mm in size) were collected at Institut Curie from 2005 to 2006 prior to any radiation, hormonal or chemotherapy treatment. Analysis of the human samples by immunohistochemistry (IHC) was performed in accordance with the French Bioethics Law 2004-800, the French National Institute of Cancer (INCa) Ethics Charter, and after approval by the Institut Curie review board and ethics committee (*Comité de Pilotage du Groupe Sein*). Patients were informed of the research use of their tissues and did not declare any opposition for such research. Tumors were classified as IBC, DCIS and microinvasive based on assessment by a pathologist [4]. Inclusion of DCIS and tumors followed same criteria as IBCs with additional marker assessment including Ki67 and p63. Microinvasive tumors were defined as infiltrating carcinomas with no invasive focus >1 mm. Tumor breast molecular subtypes were defined as follows according to the guidelines of the American Society of Clinical Oncology (ASCO)/College of American Pathologists [5, 6]: Luminal A: estrogen-receptor (ER)≥10%, progesterone-receptor (PR)≥20%, Ki-67<14%; Luminal B: ER≥10%, PR<20%, Ki-67≥14%; HER2+: ER<10%, PR<10%, HER2 2+ amplified or 3+; Triple-negative breast cancers (TNBC): ER<10%, PR<10%, HER2 0/1+ or 2+ non-amplified. The clinical and pathological features of patients are summarized in Table S2. The TMA consisted of arrayed 1-mm diameter cores from synchronous in situ and

microinvasive/invasive carcinomas and a matched core from adjacent non-tumoral breast tissue constructed as previously described [4].

Immunohistochemical (IHC) staining of breast tumor tissue microarray

Sections (3 µm) from paraffin-embedded tissue microarrays were dewaxed in xylene and rehydrated in a graded alcohol series before heat-induced antigen retrieval (60 minutes in 10 mM sodium citrate buffer, pH 6.0 at 90°C). Then, sections were incubated in 3% hydrogen peroxide solution for 5 min to inhibit endogenous peroxidase activity. The slides were further incubated with blocking serum for 15 min and then with the primary antibodies. Selective NME1 and NME2 pAbs were used: affinity-purified rabbit NME1 pAb [2] was used at a dilution of 1:3000; mouse NME2 mAb purchased from Kamiya Biomedical Company (Seattle, WA) was used at a dilution of 1:1000. Immunolabeling was performed using the Dako Autostainer Plus and EnVision™ FLEX, Low pH kit with diaminobenzidine as chromogen according to the manufacturer's procedure (Dako, Santa Clara, CA). Slides were counterstained with hematoxylin before mounting. Images were acquired with the Philips Ultra-Fast Scanner. NME1 and NME2 levels in the different tumor biopsies were scored under the supervision of a pathologist in a blinded manner using the H-score method based on semi-quantitative assessment of the intensity of plasma membrane and cytoplasmic staining (graded as: 0, non-staining; 1, weak; 2, median; or 3, strong) and the percentage of positive cells. H-score range was from 0 to 300 for membranous or cytoplasmic staining and 0 to 600 for total staining.

Unsupervised hierarchical clustering

The membranous H-score of MT1-MMP and the total H-score of NME1 from in situ

and infiltrating tumor samples were scaled and then analyzed by unsupervised hierarchical clustering using the Ward linkage clustering algorithm with Euclidean distance as the similarity metric (EMA package). Membranous MT1-MMP and total NME1 H-score variables were then discretized either in low or in high expression in order to perform association test. Cut-off values for H-scores were calculated using normal mixture modeling (Mclust R package). The same cut-off values were used for in situ and invasive components. Threshold membranous MT1-MMP: 125; threshold total NME1: 300. Membranous MT1-MMP and total NME1 H-scores were plotted as box-plot according to discretized membranous MT1-MMP and total NME1 H-scores, respectively, breast cancer subgroups, Elston and Ellis grade.

Intraductal transplantation method

The intraductal xenograft model was carried out as previously described [4, 7]. Briefly, $5x10^4$ MCF10DCIS.com cells in 2 μl PBS were injected into the primary duct through the nipples of both mammary inguinal glands #4 of 8-10 weeks-old virgin female SCID mice. Mice were sacrificed at 4 and 7 weeks after injection by cervical dislocation. Immediately after being euthanized, mammary glands were excised and processed for further study (including whole-mount and histological and IHC staining on sections). The animal facility was granted approval (C-75-12-01) given by the French Administration. All experiments were conducted according to the European Communities Council Directive (2010/63/UE) for the care and use of animals for experimental procedures and complied with the regulations of the French Ethics Committee in Animal Experiment ‘Charles Darwin’ registered at the *‘Comité National de Réflexion Ethique sur l’Experimentation Animale’* (C2EA - 05). All procedures were approved by this committee (APAFIS#11806-2017101710125048 v2).

Histological and immunofluorescence analysis of mouse tissue sections

Whole-mount carmine and hematoxylin and eosin (H&E) staining of tissue sections were performed as described in [4]. After whole mount staining, image acquisition was performed with an A1R Nikon confocal binocular microscope. Quantification of the tumor area was performed using Image J software. To retrieve antigens on paraffin-embedded tissue samples, sections were incubated for 20 min in 10 mM sodium citrate buffer, pH 6.0 at 90°C. Then, after 60 min incubation in 5% fetal calf serum, sections were incubated overnight with diluted primary antibodies, washed and further incubated for 2 hrs at room temperature with appropriate secondary antibodies.

3D collagen I invasion assay

Details of the procedure have been described [8]. Briefly, Petri dishes were filled with 1.35 ml of neutralized native type I collagen and incubated overnight at 37°C to allow gelling. Cells were harvested and isolated using Moscona buffer and trypsin/EDTA, then seeded on the top of the collagen gel at the density of 0.33 $x10^6$ cells per dish. Cells were cultured for 24 hrs in the absence or presence of GM6001 (10 μM). Non-invasive round-shape cells that remained at the surface of the gel, and invasive cells that inserted an invasive extension within the collagen gel were scored in twelve fields of 0.157 mm^2. Invasion index was calculated as the number of cells with invasive extensions to the total cell number multiplied by 100 [8].

Quantification of pericellular collagenolysis

Cells treated with siRNAs against MT1-MMP, NME1, NME2, and non-targeting siRNA for 48 hrs, or stably overexpressing NME1 (or empty vector) were trypsinized,

resuspended (2.5 x 10^5 cells/ml) in 0.2 ml of 2.2 mg/ml acidic-extracted type I collagen solution (Corning) with pH buffered to 7.5 and loaded on a glass coverslip. After gelling for 30 min at 37°C, complete medium was added and collagen-embedded cells were incubated for 24 hrs at 37°C in 5% CO_2. After fixation in 4% paraformaldehyde in PBS at 37°C for 30 min, samples were incubated with Coll-$^{3/4}$C pAb (2.5 μg/ml) for 2 hrs at 4°C, washed extensively with PBS, and counterstained with Cy3-conjugated anti-rabbit IgG antibodies, 4',6-diamidino-2-phenylindole (DAPI), and Alexa Fluor-phalloidin to visualize cell shape. Image acquisition was performed with an A1R confocal microscope (Nikon) with a 40x oil objective. Quantification of the degradation spots was performed with a home-made plugin in ImageJ [9].

Multicellular spheroid outgrowth in 3D Matrigel

For the analysis of invasive outgrowth of MCF10DCIS.om cells, an overlay basement membrane assay was performed. Briefly, 6-well plates were coated with 12 mg/ml native Matrigel and allowed to solidify for 20 min at 37°C. MCF10DCIS.com cells (3 x 10^5 cells) were seeded as single cells onto the solidified basement membrane. After 7 days, cells were imaged in triplicate for development of invasive outgrowths by differential interference contrast (DIC) imaging using a 20x objective. Invasive growths were defined as consisting of two or more cells migrating away from their structure of origin. A minimum of 20 images were analyzed for each condition.

Analysis of MT1-MMP cell surface expression

For surface detection of MT1-MMP, MCF10DCIS.com cells treated with siRNAs against NME1, NME2, and non-targeting siRNA (scrambled) for 72 hrs, ablated for NME1 and NME2 by the CRISPR/Cas9 technology, and MDA-MB-435 cells stably

overexpressing NME1 and the empty vector were cultured, collected with 5 mM EDTA in PBS with 2% BSA and surface labeled with mouse mAb against MT1-MMP (clone 2D7) and AlexaFluor-488-conjugated anti-mouse IgG secondary antibodies. Specifically, cells were blocked with 2% BSA in PBS for 1h, incubated with the primary antibody, washed three times with PBS, incubated with the secondary antibody, and washed an additional three times with PBS. To ensure surface labeling, all solutions were ice-cold and the cells were kept on ice during all incubation steps. Following staining, cells were fixed in 2% paraformaldehyde and kept in the dark until analysis. Control cells were stained in parallel with secondary antibody only to reveal background. Analysis was done using the X Flow Cytometer. The mean fluorescence intensity for control cells (secondary antibody staining only) was subtracted from the mean fluorescence intensity for each cell line population and the results are graphed as percentage of expression relative to the non-targeting siRNA or the non-targeting CRISPR/Cas9 or to the empty vector.

In situ proximity ligation assay (PLA)

To monitor the subcellular localization of protein-protein interactions at single molecule resolution, an in situ proximity ligation assay (PLA) was performed as previously described [10]. Cells grown on coverslips were fixed with cold methanol and then incubated with primary antibodies. Secondary antibodies tagged with short DNA oligonucleotides were added. Hybridization, ligation, amplification and detection were realized according to the manufacturer's protocol (Sigma-Aldrich, St. Louis, MO). Briefly, secondary antibodies were incubated in pre-heated humidity chamber for 1 hr at 37°C. Ligation was performed with a ligase-containing ligation solution for 30 min at 37°C. Finally, amplification was performed with a polymerase-containing amplification

solution for 100 min at 37°C. PLA signal corresponds to the Cy3 fluorescence. Coverslips were analyzed on an inverted wide-field microscope.

Immunoprecipitation

Cells were lysed in 50 mM Tris-HCl pH 7.5, 137 mM NaCl, 10 mM MgCl2, 10% glycerol, 1% Triton-X100 with protease inhibitors and centrifuged at 16,000*g* for 10 min at 4°C. Supernatants were incubated with 2 μg of antibody for 2 hrs at 4°C and a 1:1 mixture of Protein-A and Protein-G Sepharose 4 Fast Flow (GE Healthcare) was added and further incubated for 1 hr at 4°C. Beads were washed three times in lysis buffer, and bound proteins were eluted in SDS sample buffer and analyzed by immunoblotting with the indicated antibodies.

Subcellular fractionation

Cells were scraped and resuspended in hypotonic buffer (10 mM HEPES, pH 7.5, 2.5 mM $MgCl_2$, 2 mM EGTA with a cocktail of protease inhibitors) by repeated passages through a 27G needle. The homogenate was centrifuged at 200*g* for 10 min at 4°C to yield a post-nuclear supernatant (PNS), which was centrifuged at 100,000*g* for 60 min at 4°C to yield supernatant and pellet fractions. Pellet was resuspended in hypotonic buffer to a volume equal to the supernatant volume, and equal volume of high-speed fractions and PNS were analyzed by immunoblotting using specific antibodies. The purified clathrin-coated vesicle (CCV) fraction was kindly provided by Dr E. Smythe (University of Sheffield, UK) [11].

Production and purification of recombinant proteins

The human MT1-MMP cytosolic tail (Cter) construct for bacterial expression was produced by Genscript. The synthetic DNA coding the MT1-MMP cytosolic tail (RRHGTPRRLLYCQRSLLDKV) was inserted into pGS-21a plasmid using NcoI cloning sites. The resulting pGS-21a-MT1-MMP-Cter plasmid allowed production of MT1-MMP-Cter peptide with a cleavable by enterokinase N-terminal His-GST tag. The recombinant His-GST-MT1-MMP-Cter protein expression was performed in Escherichia coli BL21(DE3) cells. Bacterial cells were grown at 37 °C in 2xYT medium, induced at an A600 nm of OD 0.6 by the addition of 0.5 mM isopropyl-1-thio-β-D-galactopyranoside, and harvested after 18 hrs at 20°C. The cell pellet was resuspended in 50 mM Tris, pH 8.0, 150 mM NaCl, 40 mM imidazole, 1 mM TCEP and protease inhibitor mix (CLAP/cOmplete from Sigma at 1 µg/ml), lysed by sonication, and centrifuged at 35000 x *g* for 1 h. The supernatant was loaded onto a HisTrap column (GE healthcare). After washing with 20 column volumes of the wash buffer (50 mM Tris, pH 8.0, 150 mM NaCl, 40 mM imidazole, 1 mM TCEP), the protein was eluted with 250 mM imidazole. The eluted fractions with the highest protein concentration were analyzed on SDS-PAGE, the fractions containing pure His-GST-MT1-MMP-Cter were pulled and diluted 5 times in the imidazole-free buffer resulting in the 10 mg/ml protein solution that was aliquoted, frozen in liquid nitrogen and stored at -80ºC. The purified His-GST-MT1-MMP-Cter integrity was confirmed by MALDI-TOF MS analysis. Recombinant NME1 was produced as described elsewhere [12]. Purified His-GST-MT1-MMP-Cter and NME1 proteins homogeneity and oligomerization states were controlled and confirmed using size exclusion chromatography (Superdex 200) combined with multi angle light scattering (Wyatt Technology). The recombinant NME1 formed the expected hexamers.

Pull-down assay

Purified GST or GST-MT1-MMP-Cter recombinant proteins (25 μg) were immobilized on Glutathione Sepharose 4B beads (GE Healthcare) (1:1 suspension) for 1 hr at 4°C on a rotating wheel. Beads were washed three times with pulldown buffer (25 mM Tris-HCl pH 7.4, 150 mM NaCl, 5 mM $MgCl_2$, 10% (v/v) glycerol, 1% (v/v) Nonidet P-40) and subsequently incubated with purified recombinant NME1 protein (50 μg) for 2 hrs at 4°C on a rotating wheel. Beads were washed four times with pulldown buffer and bound proteins were eluted with 1x Laemmli buffer and denatured at 95°C for 30 min, and then analyzed by immunoblotting.

MT1-MMP internalization

Cells were incubated for 1 hr on ice in the presence of 0.5 mg/ml NHS-SS-biotin (Pierce Chemical, Rockford, IL). Labeled cells were then washed and incubated at 37°C for 1 hr to allow for internalization of surface proteins. Samples were then washed and treated successively (20 min at 4°C) with a reducing solution (42 mM glutathione, 75 mM NaCl, 1 mM EDTA, 1% bovine serum albumin, and 75 mM NaOH) to strip biotinylated proteins from the cell surface. After a final wash, cells were lysed in 10 mM Tris, pH 7.2, 150 mM NaCl, 1 mM $CaCl_2$, 1 mM $MgCl_2$, and 1 % Nonidet P-40. Biotinylated proteins were captured with streptavidin-Sepharose beads (Pierce Chemical), and recovered complexes were resolved under reducing conditions by SDS-PAGE followed by Western blot analysis. The total pool of biotinylated MT1-MMP was determined in samples where the incubation step with the reducing solution was omitted [13].

Statistical analysis

Analyses were performed using R software, 3.5.0 version (http://cran.rproject.org). Boxplots were generated with the R ggplot2 package. All statistical tests were two-sided. *P* values of 0.05 or below were considered significant. Comparison of H-scores between matched in situ and invasive or microinvasive lesions was performed using paired Student's t-test. Comparison of H-scores between two different breast molecular subtypes was performed using Welch two samples t-test (Welch's t-test is an adaptation of the Student's t-test and is more reliable when the two independent samples have unequal sample sizes). Membranous MT1-MMP and total NME1 H-scores were compared between groups by ANOVA test. Comparison of in situ or invasive tumors in glands injected with "NT", "KO NME1(#A)", "KO NME1(#B)", "KO NME2(#A)" or "KO NME2(#B)" clones was performed using the Chi2 test. The distributions of tumor area (mm^2) in mammary glands in mice injected with "NT", "KO NME1(#A)", "KO NME1(#B)", "KO NME2(#A)" or "KO NME2(#B)" clones were compared using a non-parametric method by ranks (Kruskall-Wallis test) because of small sample size. Comparisons were also performed according to the tumor type (in situ or invasive tumor, respectively). For all other comparisons, the unpaired Student's t-test was used.

Supplemental references

1 Hotary K, Allen E, Punturieri A, Yana I, Weiss SJ. Regulation of cell invasion and morphogenesis in a three-dimensional type I collagen matrix by membrane-type matrix metalloproteinases 1, 2, and 3. *J Cell Biol* 2000; 149: 1309-1323.

2 Boissan M, Wendum D, Arnaud-Dabernat S, Munier A, Debray M, Lascu I *et al*. Increased lung metastasis in transgenic NM23-Null/SV40 mice with hepatocellular carcinoma. *J Natl Cancer Inst* 2005; 97: 836-845.

3 Chenard MP, Lutz Y, Mechine-Neuville A, Stoll I, Bellocq JP, Rio MC *et al*. Presence of high levels of MT1-MMP protein in fibroblastic cells of human invasive carcinomas. *Int J Cancer* 1999; 82: 208-212.

4 Lodillinsky C, Infante E, Guichard A, Chaligne R, Fuhrmann L, Cyrta J *et al*. p63/MT1-MMP axis is required for in situ to invasive transition in basal-like breast cancer. *Oncogene* 2016; 35: 344-357.

5 Prat A, Cheang MC, Martin M, Parker JS, Carrasco E, Caballero R *et al*. Prognostic significance of progesterone receptor-positive tumor cells within immunohistochemically defined luminal A breast cancer. *J Clin Oncol* 2013; 31: 203-209.

6 Wolff AC, Hammond ME, Schwartz JN, Hagerty KL, Allred DC, Cote RJ *et al*. American Society of Clinical Oncology/College of American Pathologists

guideline recommendations for human epidermal growth factor receptor 2 testing in breast cancer. *Arch Pathol Lab Med* 2007; 131: 18-43.

7 Behbod F, Kittrell FS, LaMarca H, Edwards D, Kerbawy S, Heestand JC *et al*. An intraductal human-in-mouse transplantation model mimics the subtypes of ductal carcinoma in situ. *Breast Cancer Res* 2009; 11: R66.

8 De Wever O, Hendrix A, De Boeck A, Westbroek W, Braems G, Emami S *et al*. Modeling and quantification of cancer cell invasion through collagen type I matrices. *Int J Dev Biol* 2010; 54: 887-896.

9 Monteiro P, Rosse C, Castro-Castro A, Irondelle M, Lagoutte E, Paul-Gilloteaux P *et al*. Endosomal WASH and exocyst complexes control exocytosis of MT1-MMP at invadopodia. *J Cell Biol* 2013; 203: 1063-1079.

10 Soderberg O, Gullberg M, Jarvius M, Ridderstrale K, Leuchowius KJ, Jarvius J *et al*. Direct observation of individual endogenous protein complexes in situ by proximity ligation. *Nat Methods* 2006; 3: 995-1000.

11 Semerdjieva S, Shortt B, Maxwell E, Singh S, Fonarev P, Hansen J *et al*. Coordinated regulation of AP2 uncoating from clathrin-coated vesicles by rab5 and hRME-6. *J Cell Biol* 2008; 183: 499-511.

12 Mocan I, Georgescauld F, Gonin P, Thoraval D, Cervoni L, Giartosio A *et al*. Protein phosphorylation corrects the folding defect of the neuroblastoma

(S120G) mutant of human nucleoside diphosphate kinase A/Nm23-H1. *Biochem J* 2007; 403: 149-156.

13 Li XY, Ota I, Yana I, Sabeh F, Weiss SJ. Molecular dissection of the structural machinery underlying the tissue-invasive activity of membrane type-1 matrix metalloproteinase. *Mol Biol Cell* 2008; 19: 3221-3233.

Supplemental Figure legends

Supplemental Figure S1. Specificity validation of NME1 and -NME2 antibodies

(A) Left panel: NME1 expression was analyzed by immunoblotting using home-made NME1 pAb in MDA-MB-435 and MDA-MB-231 cells stably overexpressing NME1 (NME1) or in cells transfected with a control vector (CTRL), and in MCF10DCIS.com cells treated with a NME1-targeting siRNA (siNME1) or scramble siRNA (Scr). Right panel: the same samples were analyzed with NME1 mAb from OriGene. (**B**) Enzyme-linked immunosorbent assay (ELISA) using purified recombinant human $NME1_r$ or $NME2_r$ proteins and 10^{-3}, 10^{-4} and 10^{-5} dilutions of NME2 mAb (Kamiya Biomedical Company). **(C)** Western blotting analysis using purified recombinant human $NME1_r$, $NME2_r$, $NME3_r$ or $NME4_r$ proteins revealed with NME2 mAb as in B. **(D)** Western blotting analysis of HeLa cell lysates silenced for NME2 or scramble siRNA-treated (Scr) with NME2 mAb as in B. Alpha-tubulin was used as a loading control. Molecular weights are in kDa.

Supplemental Figure S2. NME1 expression in synchronous in situ and invasive components of breast tumors

(A-B) Representative IHC staining of NME1 in breast peritumoral tissues and in synchronous in situ and invasive components from two breast carcinoma biopsies using home-made NME1 pAb. Arrowheads point to plasma membrane NME1 staining. Scale bar, 50 μm.

Supplemental Figure S3. NME1 is downregulated in invasive relative to synchronous in situ components irrespective of the breast cancer subgroup

(A-C) Comparison of NME1 levels using the H-score method in in situ and invasive components of the breast cancer cohort (N=156 breast tumor clinical specimens) segregated in the different Luminal A & B, HER2+ and TNBC subgroups. The median of each H-score distribution is represented (red bar). **(D, E)** Comparison of NME1 levels in the in situ (D) or invasive components (E) of Luminal A & B and TNBC breast carcinomas. *** $P < 0.001$; * $P < 0.05$. The median of each H-score distribution is represented (red bar).

Supplemental Figure S4. Confirmation of biphasic up- and down-regulation of NME1 expression using NME1 mAb from OriGene

(A-B) Representative IHC staining of NME1 in breast peritumoral tissues and in synchronous in situ and invasive components from two breast carcinoma biopsies using Origene NME1 mAb. Scale bar, 25 μm.

Supplemental Figure S5. NME1 expression is downregulated in microinvasive breast carcinomas

(A-B) Two representative examples of NME1 IHC staining of synchronous in situ and microinvasive breast carcinomas. Arrowheads point to plasma membrane staining. Scale bar, 50 μm. **(C-E)** Comparison of total (C), cytoplasmic (D) and plasma membrane (E) NME1 levels (H-score) in synchronous in situ and microinvasive breast carcinomas. *** $P < 0.001$; ** $P < 0.01$. The median of each H-score distribution is represented (red bar).

Supplemental Figure S6. Up-regulation of NME2 in breast cancer

(A-B) Representative NME2 IHC staining in breast peritumoral tissues and synchronous in situ and invasive components from two breast carcinoma biopsies. Arrows point to NME2 apical staining in peritumoral epithelial tissue. Arrowheads point to plasma membrane staining in breast carcinoma cells. Scale bar, 25 μm. (**C, E and G**) Comparison of total (C), cytoplasmic (E) and plasma membrane (G) NME2 levels using the H-score method in in situ breast carcinomas as compared to adjacent peritumoral tissues. *** $P < 0.001$; ns, not significant. **(D, F and H)** NME2 levels were compared in synchronous in situ and invasive components of breast tumor biopsies. ns, not significant. The median of each H-score distribution is represented (red bar).

Supplemental Figure S7. Additional examples of anti-correlated NME1 and MT1-MMP staining in human breast tumors

(A, B) Representative immunostaining of serial sections of synchronous in situ (A) and invasive (B) components of human breast carcinoma (case #2) using NME1 pAb and MT1-MMP mAb. Tumor foci are delineated by a dashed line. Scale bar, 25 μm.

Supplemental Figure S8. Definition of cut-off values for membranous MT1-MMP and total NME1 H-score variables in the overall breast cancer cohort

(A-D) Cut-off values for membranous MT1-MMP and total NME1 H-score variables were calculated using normal mixture modeling in in situ (A, B) and invasive (C, D) components of the overall human breast tumor cohort. The same cut-off values were used for in situ and invasive components. Threshold membranous MT1-MMP: 125; threshold total NME1: 300.

Supplemental Figure S9. Validation of NME1 and NME2 knockout in MCF10DCIS.com clones

Fraction of sequencing reads aligned to the reference amplicon sequence and for which an insertion or deletion was observed. For both NME1 and NME2 genes, two sites (referred to as A and B) were targeted for edition by CRISPR/Cas9 in MCF10DCIS.com cells. Corresponding targeted sites were sequenced after amplification with appropriate primers (see Table S1). Top labels refer to the different MCF10DCIS.com cell populations. Bar colors and x axis labels refer to the amplicon. Parental, MCF10DCIS.com cells not subjected to CRISPR/Cas9 edition; NT, MCF10DCIS.com cells not targeted, i.e. cells subjected to CRISPR/Cas9 edition with no guide; KO NME1(#A) and (#B), MCF10DCIS.com cells subjected to CRISPR/Cas9 edition of NME1 gene for which two sites A and B were targeted, respectively; KO NME2(#A) and (#B), MCF10DCIS.com cells subjected to CRISPR/Cas9 edition of NME2 gene for which two sites A and B were targeted, respectively.

Supplemental Figure S10. Increased proliferation rate in NME2 knockout intraductal tumor xenografts

(A) Cell proliferation marker, PCNA, (green) and DAPI (blue) immunofluorescence staining of intraductal tumor xenograft tissue sections of control (NT) and knockout MCF10DCIS.com clones. Analysis was performed 4 weeks after nipple injection. Scale bar, 50 μm. **B)** The percentage of PCNA-positive nuclei was determined from three different fields from three independent tumors. Error bars are the standard error of the mean (SEM). *** $P < 0.001$.

Supplemental Figure S11. Validation of MT1-MMP surface labeling by FACS

(A, C) Lysates of MCF10DCIS.com cells knockdown for MT1-MMP upon shRNA expression (A) or overexpressing MT1-MMPmCherry (C) were analyzed by immunoblotting with MT1-MMP mAb. Mock-treated (A) or parental (C) MCF10DCIS.com cell lysates were used as control. Molecular weights are in kDa. **(B, D)** Representative FACS profiles generated by surface MT1-MMP labeling in cells silenced (A) or overexpressing (C) MT1-MMP as compared to control cells (continuous line).

Supplemental Figure S12. Immunoblotting analysis of MT1-MMP expression in knockdown cells

(A) Lysates of control non-KO MCF10DCIS.com cells (NT) or of two independent clones knockout for NME1 or NME2 treated (+) or not (-) with MT1-MMP siRNA were analyzed by immunoblotting with the anti-MT1-MMP antibodies. Alpha-tubulin was used as a loading control. **(B)** Lysates of MCF10DCIS.com cells treated with control scrambled siRNA (Scr), or siRNA specific for NME1 or MT1-MMP were analyzed by immunoblotting with the indicated antibodies. GAPDH was used as a loading control. Molecular weights are in kDa.

Supplemental Figure S13. Cell fractionation and co-immunoprecipitation analysis of NME2

(A) After homogenization, a post-nuclear supernatant (PNS) of MCF10DCIS.com cells was ultracentrifuged to produce soluble (Supernatant) and membrane (Pellet) fractions. Proteins corresponding to equivalent cell-number were loaded in each lane and analyzed by immunoblotting with the indicated antibodies. The transferrin receptor (TfR) and the α-adaptin subunit of the AP-2 clathrin adaptor complex were recovered

in the membrane pellet fraction. NME2 partitioned both in the cytosolic and membrane fractions similar to NME1 (see Figure 4A). **(B)** PNS and clathrin-coated vesicle (CCV) fractions (10 μg) isolated from porcine brain were analyzed by immunoblotting with the indicated antibodies. **(C)** Lysates of control MCF10DCIS.com cells or cells knocked out for NME2 (clone #A and #B) were immunoprecipitated with NME2 antibodies or control IgGs followed by immunoblotting analysis with MT1-MMP antibodies. 1% of total lysate was loaded as a control (input). Molecular weight markers are indicated (in kDa).

Primer name	Adapter sequence	Locus specific primer sequence
NME1A-Fwd	TCGTCGGCAGCGTCAGATGTGTATAAGAGACAG	AATAGTTGCCAGATTTTCTGCTGT
NME1A-Rev	GTCTCGTGGGCTCGGAGATGTGTATAAGAGACAG	GGGAAAAATACCAAAATCTCACCT
NME1B-Fwd	TCGTCGGCAGCGTCAGATGTGTATAAGAGACAG	CAGTGTGGAGAATGAATTGGGTTA
NME1B-Rev	GTCTCGTGGGCTCGGAGATGTGTATAAGAGACAG	AGTATCCCACACAGGCACACTC
NME2A-Fwd	TCGTCGGCAGCGTCAGATGTGTATAAGAGACAG	GCGTGGTGGGGGAGGAG
NME2A-Rev	GTCTCGTGGGCTCGGAGATGTGTATAAGAGACAG	GGAGACGGGGGCGAGTTACC
NME2B-Fwd	TCGTCGGCAGCGTCAGATGTGTATAAGAGACAG	GACTTGCTAATGGGAGGTTCAGAG
NME2B-Rev	GTCTCGTGGGCTCGGAGATGTGTATAAGAGACAG	CAAAGAACACTGAGCACTTTTTCC

Table S1: Nextera XT adapter overhangs sequences and locus specific primer sequences used for the edition of NME1 and NME2 genes by CRISPR/Cas9.
For both NME1 and NME2 genes, two sites (referred to as A and B) were targeted for edition by CRISPR/Cas9 in MCF10DCIS.com cells. Corresponding targeted sites were sequenced after amplification with appropriate primers.

FEATURES	Invasive carcinoma (n=156)	Microinvasive carcinoma (n=37)
Age (years)		
≤ 50	72 (46,2%)	9 (24,3%)
> 50	84 (53,9%)	28 (75,7%)
Menopausal status		
Premenopausal	63 (40,4%)	9 (24,3%)
Postmenopausal	81 (51,9%)	26 (70,3%)
Unknown	12 (7,7%)	2 (8,1%)
Histological grade (invasive tumors)		
I	28 (18%)	x
II	60 (38,5%)	x
III	66 (42,3%)	x
Unknown	2 (1,3%)	x
Nuclear grade (CCIS & Mic)		
High	x	30 (81,1%)
Non high	x	7 (18,9%)
Histological subtype		
Ductal carcinoma	152 (97,5%)	x
Others	4 (2,5%)	x
Tumour size (cm)		
Tis	x	x
T1mic	x	37 (100%)
T1 (<2)	114 (73,1%)	x
T2 (2 - 5)	36 (23,1%)	x
T3 (>5)	6 (3,9%)	x
N stage		
N0	79 (50,6%)	x
N1	51 (32,7%)	x
N2	20 (12,8%)	x
N3	4 (2,6%)	x
Unknown	2 (1,3%)	x
ER		
Positive	93 (59,6%)	18 (48,6%)
Negative	63 (40,4%)	19 (51,4%)
PR		
Positive	81 (51,9%)	14 (37,9%)
Negative	74 (47,4%)	23 (62,1%)
Unknown	1 (0,7%)	x
HER2		
Positive	43 (27,6%)	15 (40,6%)
Negative	113 (72,5%)	22 (59,4%)
Ki67		
Positive (>20%)	111 (71,2%)	25 (67,6%)
Negative (<20%)	44 (28,2%)	12 (32,4%)
Unknown	1 (0,7%)	x
Molecular subtype		
TNBC	23 (14,8%)	3 (8,1%)

HER2	39 (25%)	14 (37,8%)
Luminal A	49 (31,4%)	8 (21,6%)
Luminal B	41 (26,3%)	8 (21,6%)
Luminal B / HER2	4 (2,6%)	4 (10,8%)

Table S2: Clinicopathological parameters of 156 invasive breast tumors and 37 microinvasive breast tumors

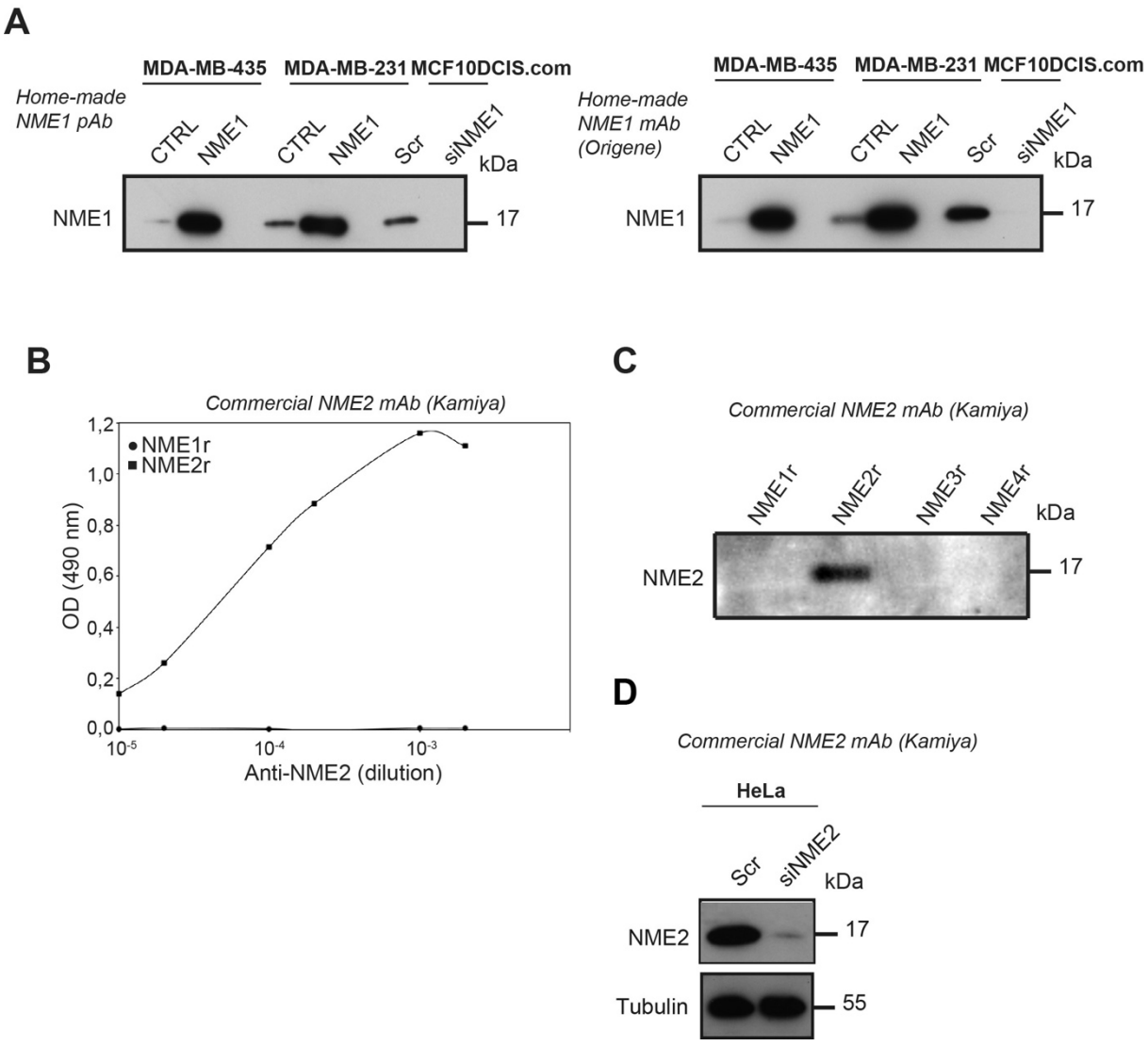
A
MDA-MB-435
MDA-MB-231
MCF10DCIS.com
Home-made NME1 pAb
CTRL
NME1
CTRL
NME1
Scr
siNME1
kDa
NME1
17
Home-made NME1 mAb (Origene)
B
Commercial NME2 mAb (Kamiya)
NME1r
NME2r
OD (490 nm)
Anti-NME2 (dilution)
C
Commercial NME2 mAb (Kamiya)
NME1r
NME2r
NME3r
NME4r
NME2
D
Commercial NME2 mAb (Kamiya)
HeLa
Scr
siNME2
Tubulin
55

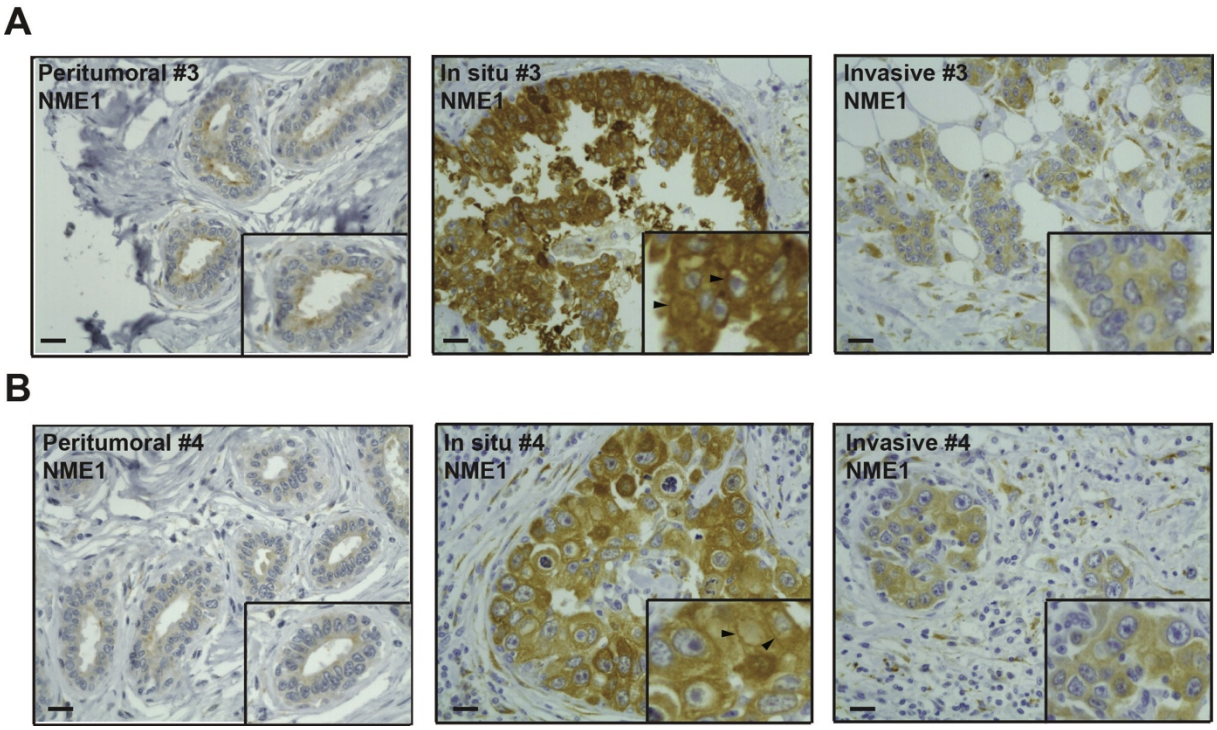
A
Peritumoral #3
NME1
In situ #3
NME1
Invasive #3
NME1
B
Peritumoral #4
NME1
In situ #4
NME1
Invasive #4
NME1

Supplemental Figure 3

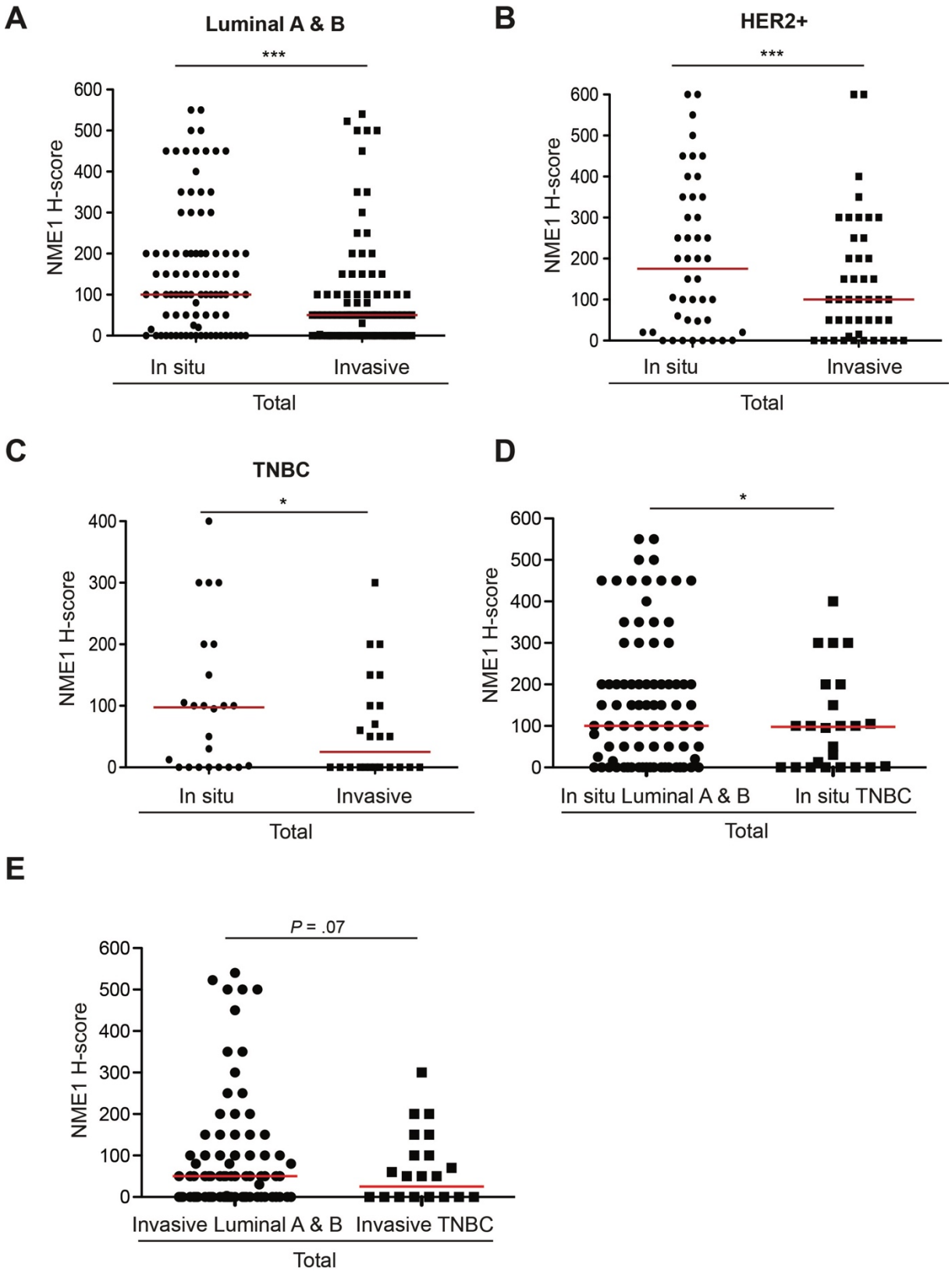

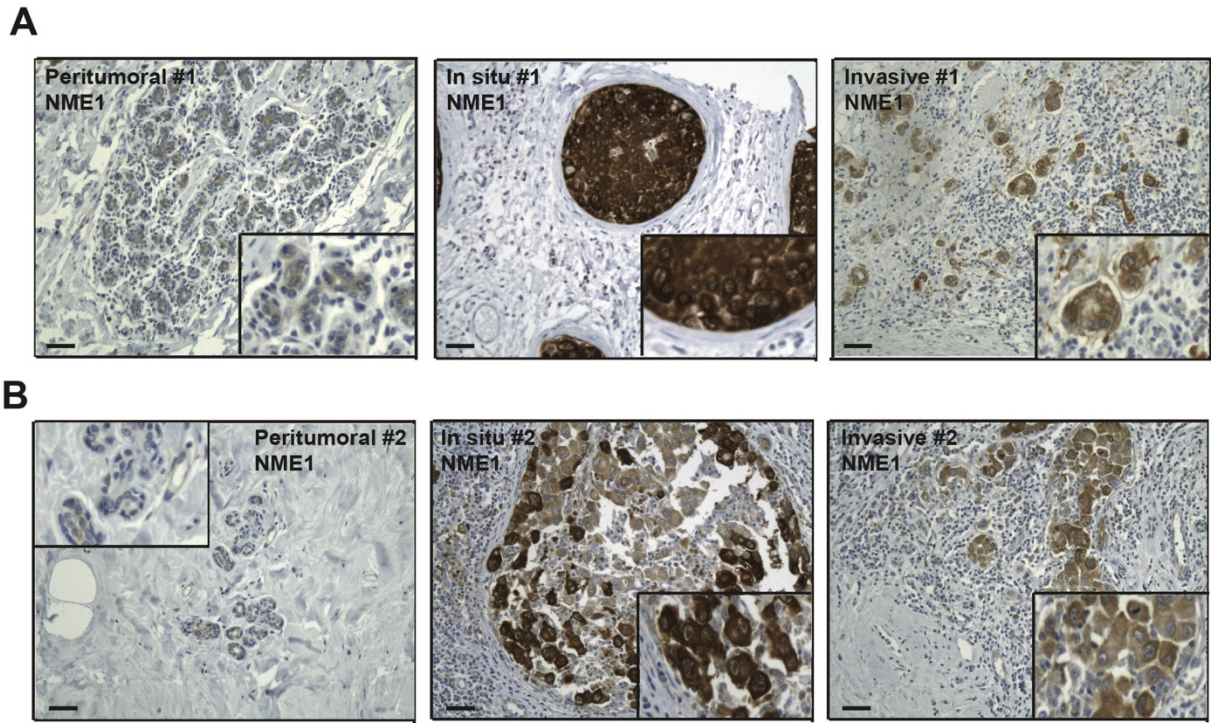
A
Peritumoral #1
NME1
In situ #1
NME1
Invasive #1
NME1
B
Peritumoral #2
NME1
In situ #2
NME1
Invasive #2
NME1

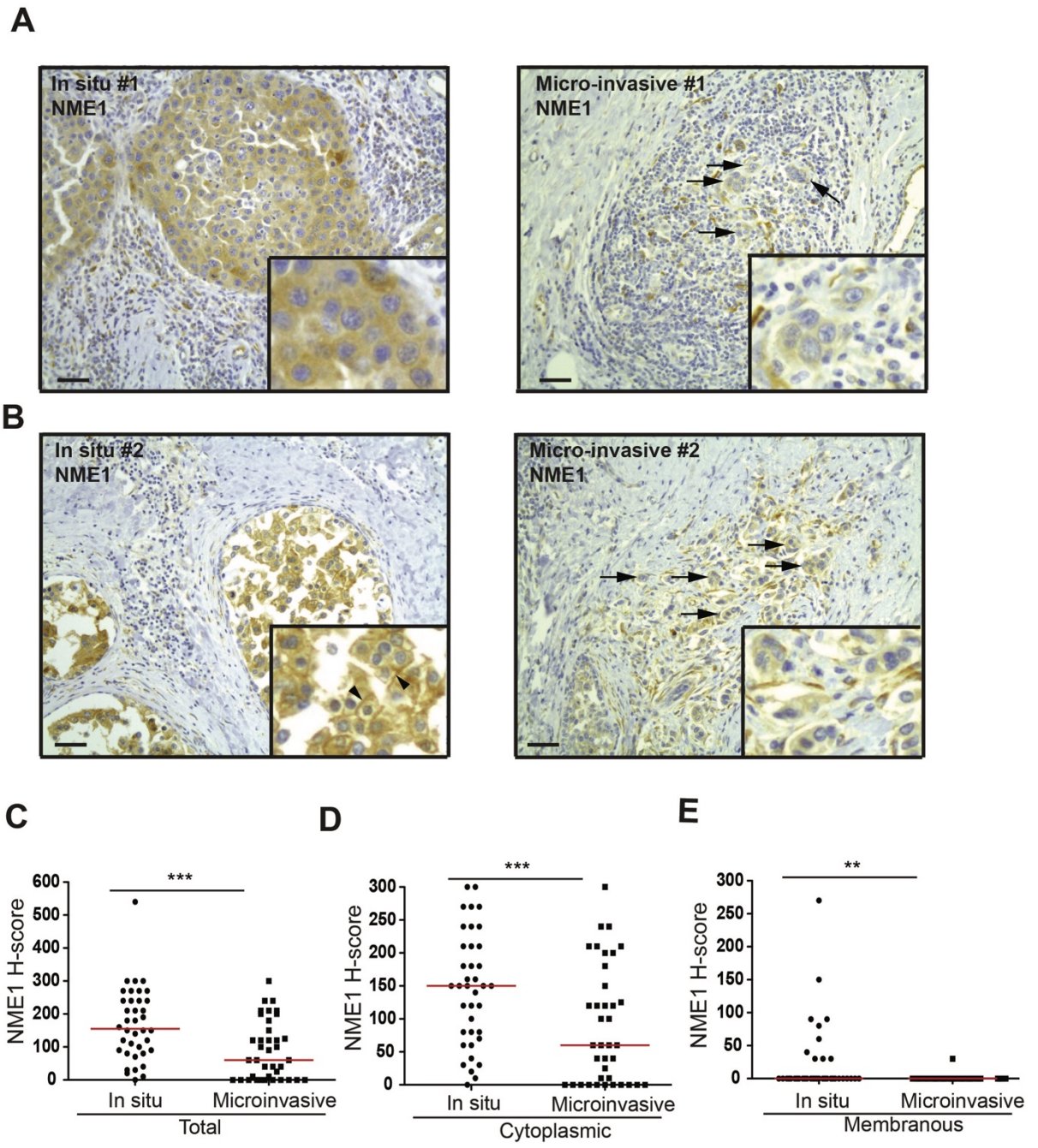
A
In situ #1
NME1
Micro-invasive #1
NME1
B
In situ #2
NME1
Micro-invasive #2
NME1
C
NME1 H-score
600
500
400
300
200
100
0
***
In situ
Microinvasive
Total
D
NME1 H-score
300
250
200
150
100
50
0
***
In situ
Microinvasive
Cytoplasmic
E
NME1 H-score
300
250
200
150
100
50
0
**
In situ
Microinvasive
Membranous

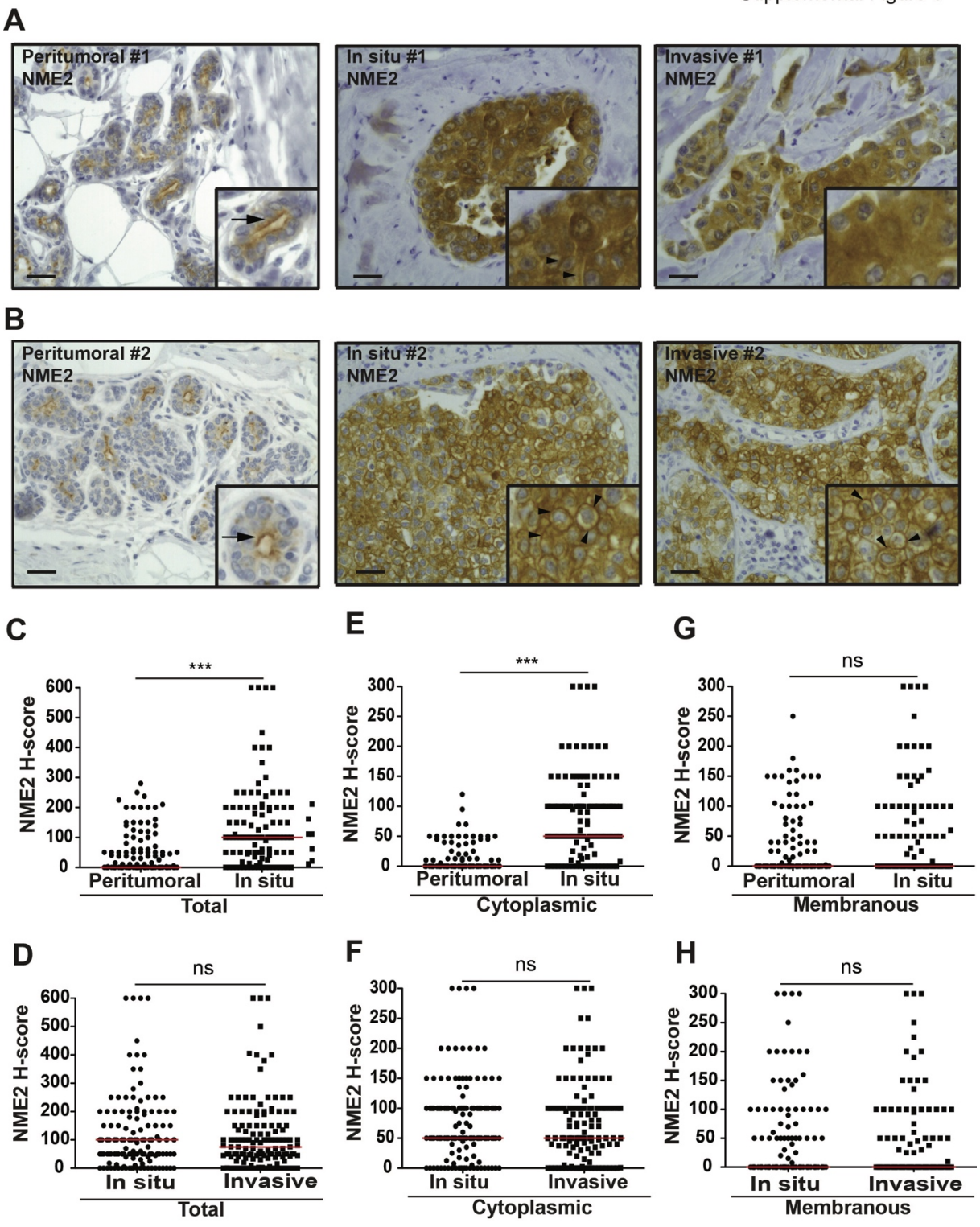
A
Peritumoral #1
NME2
In situ #1
NME2
Invasive #1
NME2
B
Peritumoral #2
NME2
In situ #2
NME2
Invasive #2
NME2
C
***
NME2 H-score
600
500
400
300
200
100
0
Peritumoral
In situ
Total
E
***
NME2 H-score
300
250
200
150
100
50
0
Peritumoral
In situ
Cytoplasmic
G
ns
NME2 H-score
300
250
200
150
100
50
0
Peritumoral
In situ
Membranous
D
ns
NME2 H-score
600
500
400
300
200
100
0
In situ
Invasive
Total
F
ns
NME2 H-score
300
250
200
150
100
50
0
In situ
Invasive
Cytoplasmic
H
ns
NME2 H-score
300
250
200
150
100
50
0
In situ
Invasive
Membranous

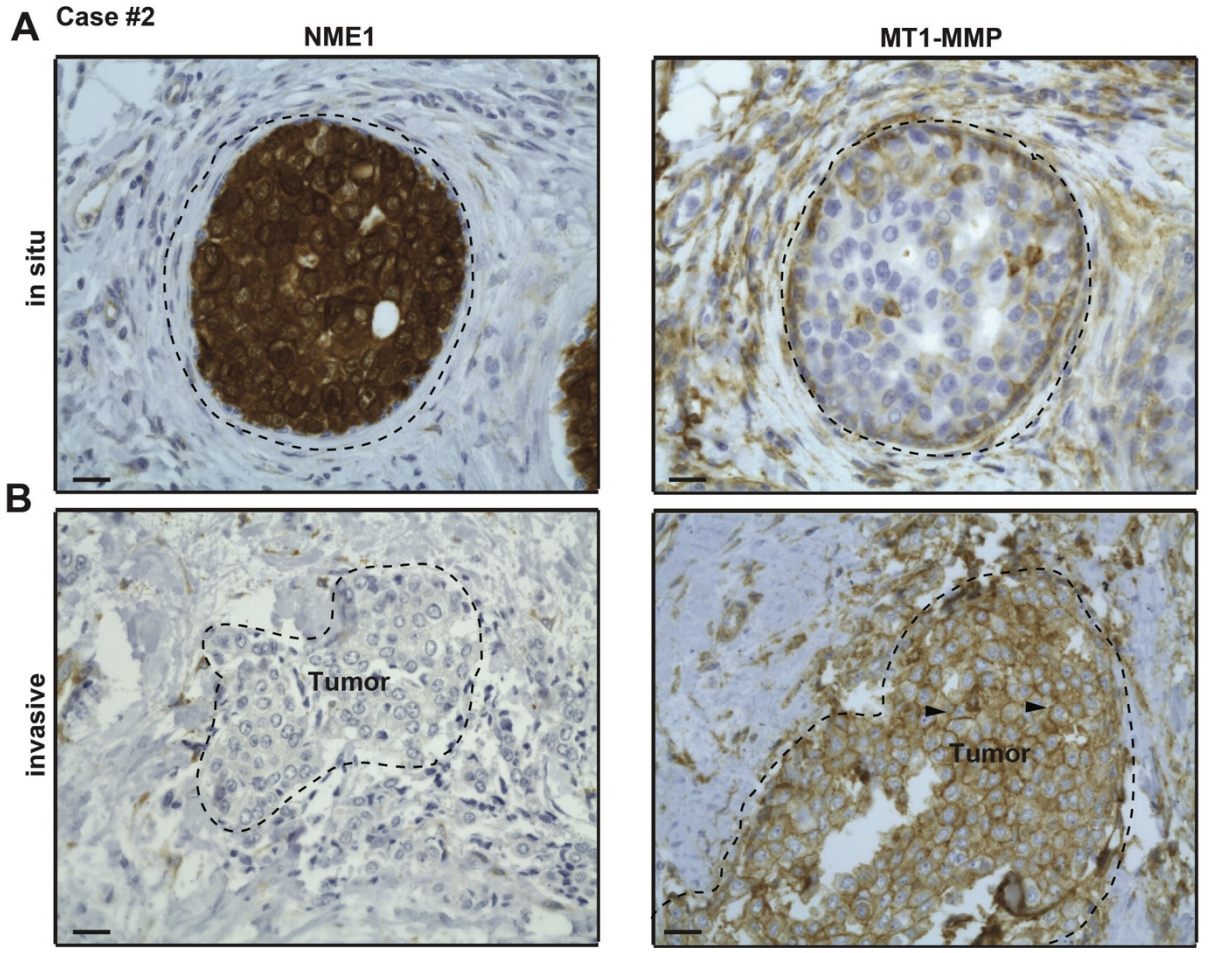
A
Case #2
NME1
MT1-MMP
in situ
B
invasive
Tumor
Tumor

Supplemental Figure 8

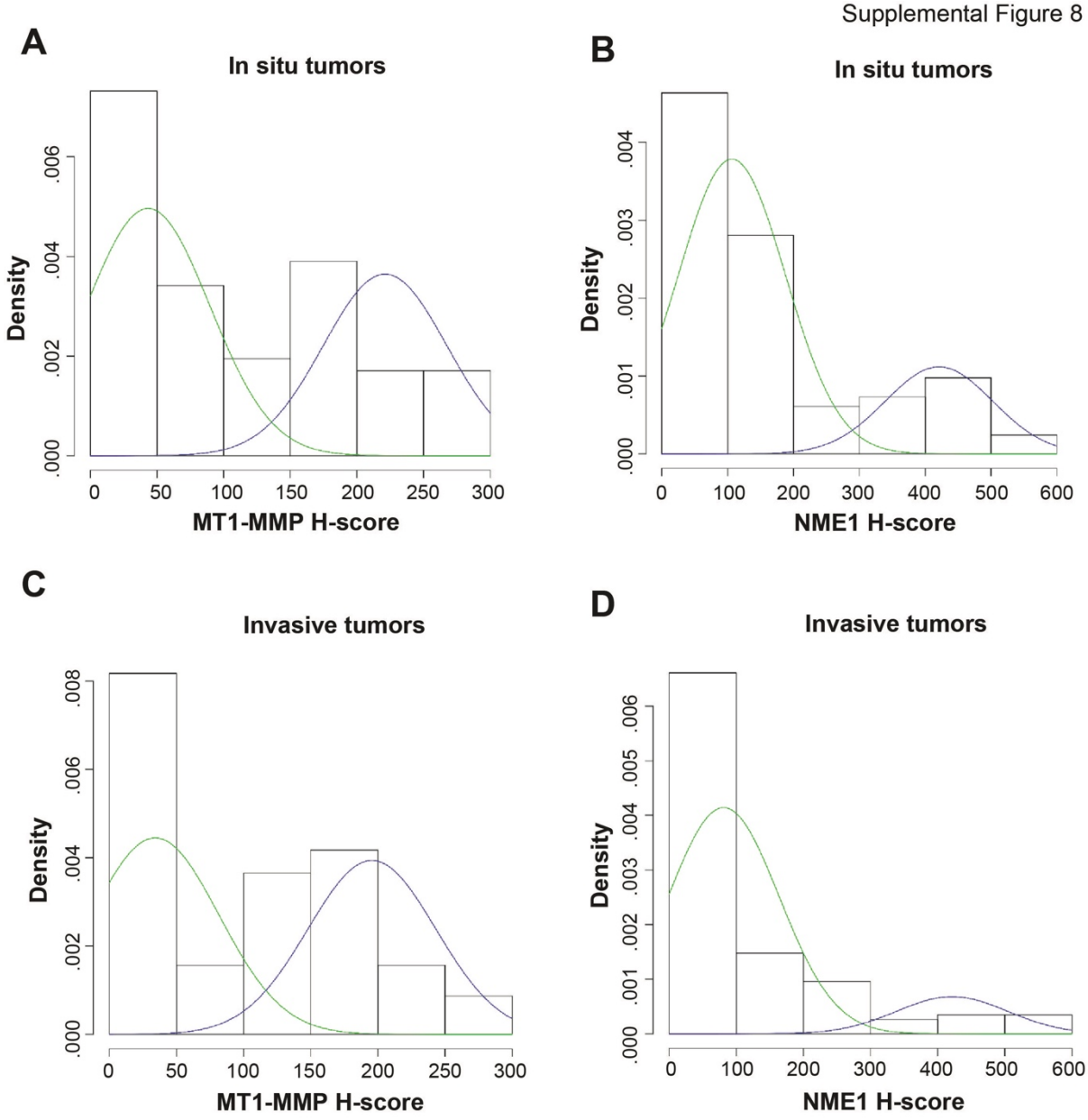

Supplemental Figure 9

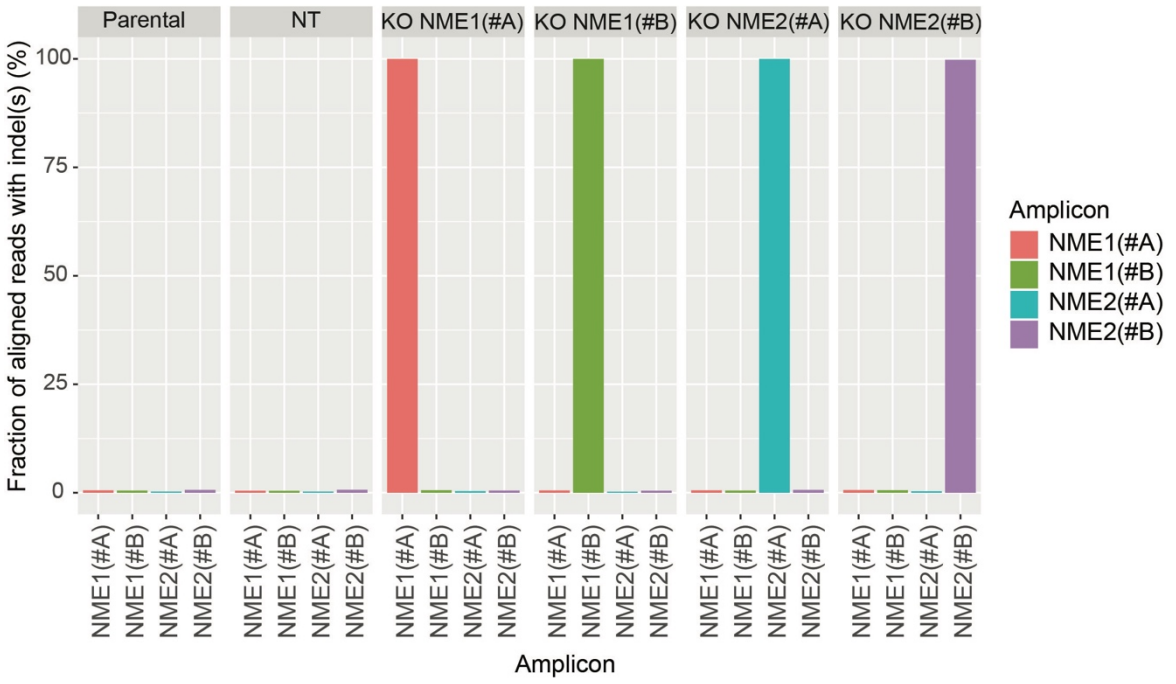

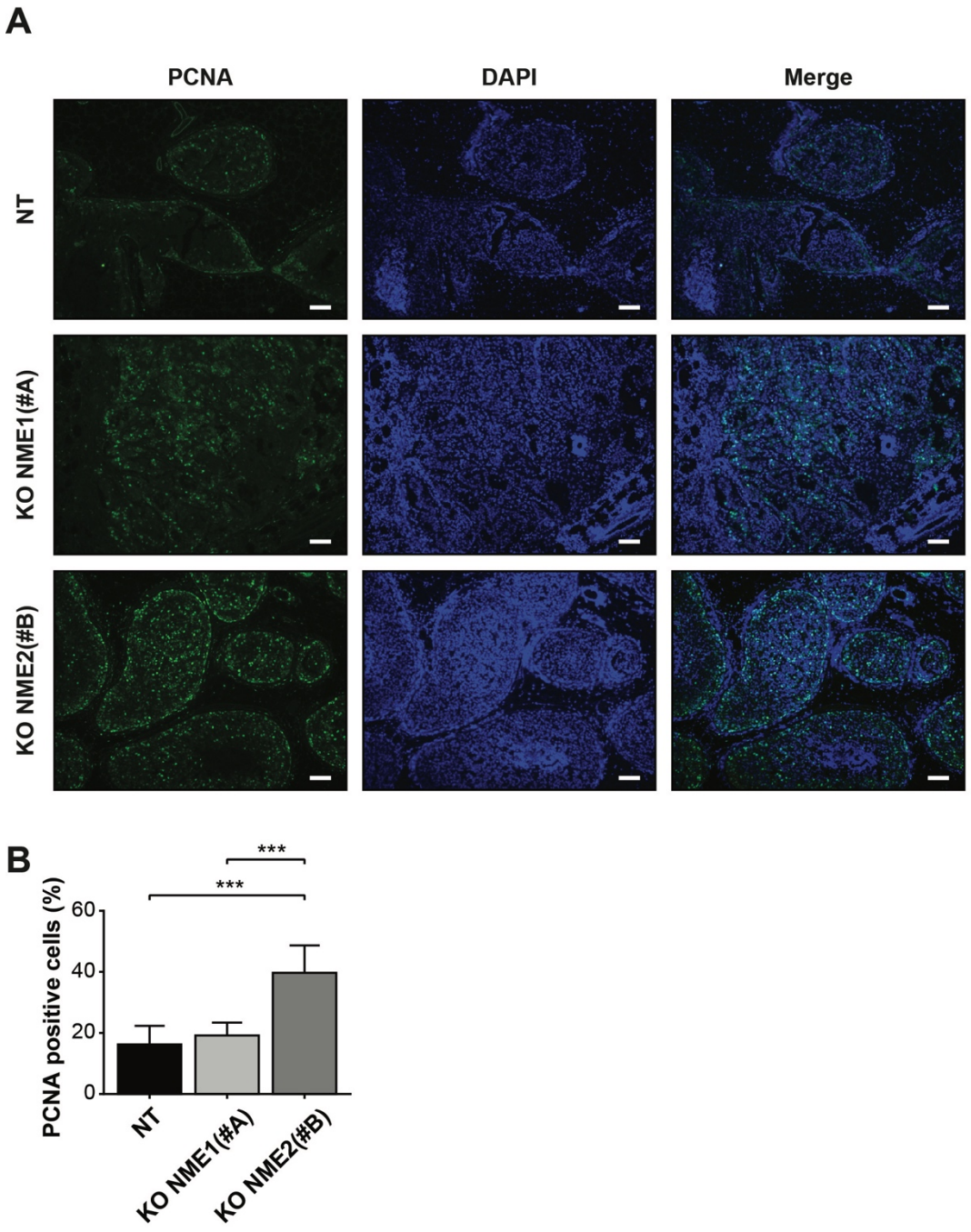
A
PCNA
DAPI
Merge
NT
KO NME1(#A)
KO NME2(#B)
B
PCNA positive cells (%)
60
40
20
0
***
***
NT
KO NME1(#A)
KO NME2(#B)

Supplemental Figure 11

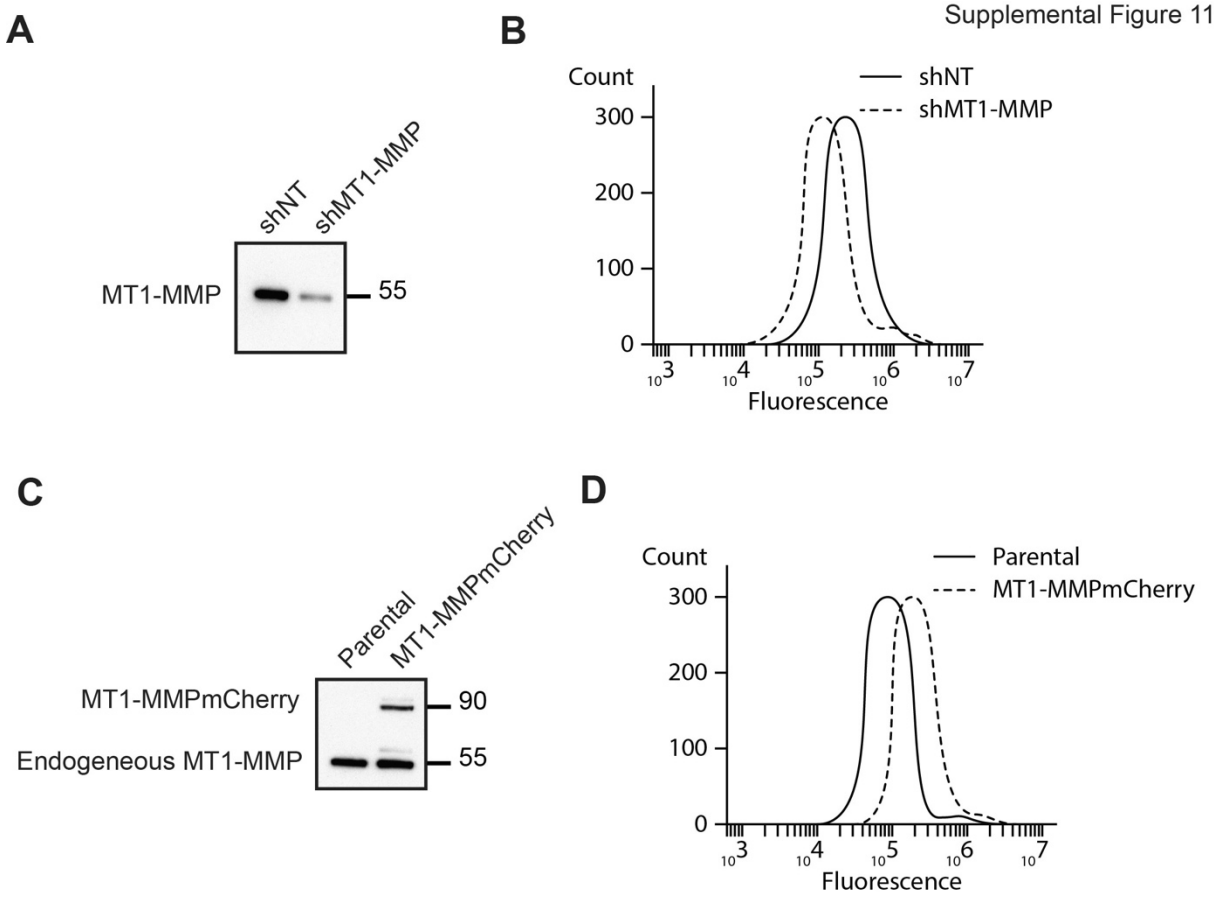

Supplemental Figure 12

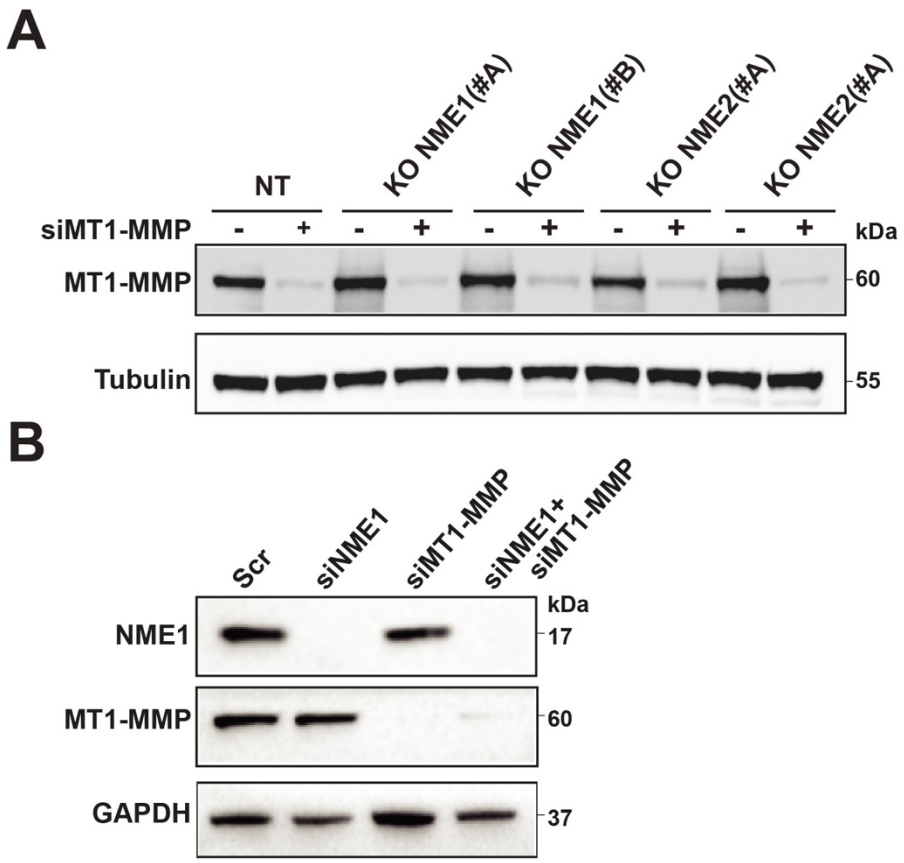

Supplemental Figure 13